Article

Spectroscopic and Computational Studies of Co-Corrinoids: Spectral and Electronic Properties of the B Cofactors and Biologically Relevant Precursors

Troy A. Stich, Amanda J. Brooks, Nicole R. Buan, and Thomas C. Brunold

J. Am. Chem. Soc., **2003**, 125 (19), 5897-5914• DOI: 10.1021/ja029328d • Publication Date (Web): 22 April 2003

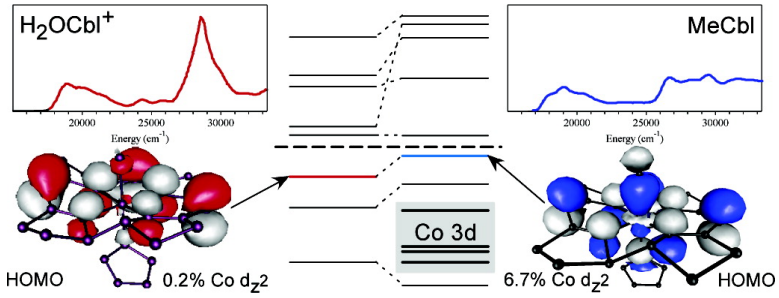

More About This Article

Additional resources and features associated with this article are available within the HTML version:

- Supporting Information
- Links to the 11 articles that cite this article, as of the time of this article download
- Access to high resolution figures
- Links to articles and content related to this article
- Copyright permission to reproduce figures and/or text from this article

View the Full Text HTML

J|A|C|S
ARTICLES
Published on Web 04/22/2003

Spectroscopic and Computational Studies of Co^{3+}-Corrinoids: Spectral and Electronic Properties of the B_{12} Cofactors and Biologically Relevant Precursors

Troy A. Stich, Amanda J. Brooks, Nicole R. Buan,† and Thomas C. Brunold*

Contribution from the Department of Chemistry, University of Wisconsin-Madison, Madison, Wisconsin 53706

Received November 13, 2002; E-mail: brunold@chem.wisc.edu

Abstract: The B_{12} cofactors methylcobalamin (MeCbl) and 5′-deoxyadenosylcobalamin (AdoCbl) have long fascinated chemists because of their complex structures and unusual reactivities in biological systems; however, their electronic absorption (Abs) spectra have remained largely unassigned. In this study, we have used Abs, circular dichroism (CD), magnetic CD (MCD), and resonance Raman spectroscopic techniques to probe the electronic excited states of Co^{3+}Cbl species that differ with respect to their upper axial ligand, including MeCbl, AdoCbl, aquacobalamin (H_2OCbl^+), and vitamin B_{12} (cyanocobalamin, CNCbl). Also included to probe the effect of the lower axial ligand on the electronic properties of Cbls is Adocobinamide ($AdoCbi^+$), an AdoCbl derivative that lacks the tethered base 5,6-dimethylbenzimidazole (DMB) and instead binds a water molecule in the lower axial position. Spectroscopic data for each species are analyzed within the framework of time-dependent density functional theory (TD-DFT) to assign the major spectral features (the so-called α/β, D/E, and γ bands) and to generate experimentally validated electronic-structure descriptions. These studies reveal that the "unique" Abs spectra of MeCbl and AdoCbl, which differ considerably from the "typical" Abs spectra of H_2OCbl^+ and CNCbl, reflect the high degree of σ-donation from the alkyl ligand to the Co center and the consequent destabilization of all Co 3d orbitals. They reveal further that with increasing σ-donor strength of the upper axial ligand, the contribution from the formally unoccupied Co $3d_{z^2}$ orbital to the HOMO increases, which induces a strong $Co-N_{DMB}$ σ-antibonding interaction, consistent with the experimentally observed lengthening of this bond from H_2OCbl^+ to CNCbl and MeCbl. Alternatively, our spectroscopic and computational data for MeCbl and $MeCbi^+$ reveal that substitution of the DMB by a water molecule in the lower axial position has negligible effects on the Co−C bond. A simple model is presented that explains why the identity of the upper axial ligand has a major effect on the $Co-N_{ax}$ bond strength, whereas the lower axial ligand does not appreciably modulate the nature of the Co−C bond. Implications of these results with respect to enzymatic Co−C bond activation are discussed.

1. Introduction

The B_{12} cofactors methylcobalamin (MeCbl) and 5′-deoxyadenosylcobalamin (AdoCbl) have fascinated chemists for over 60 years with their complex structures (Figure 1) and unusual reactivities in biological systems.[1−5] Each cobalamin possesses a low-spin Co^{3+} center ligated equatorially by the four nitrogens of a highly substituted macrocycle (the corrin ring) and axially coordinated by a nitrogen from the tethered base 5,6-dimethylbenzimidazole (DMB).[6] A wide range of ligands can occupy the upper axial position, such as CN, H_2O, Me, and Ado; however, only MeCbl and AdoCbl are enzymatically competent.[7,8] The MeCbl-dependent enzymes (e.g., methionine synthase) catalyze methyl-transfer reactions in which the cofactor's Co−C bond is cleaved heterolytically, leaving behind a protein-bound Co^{1+} cobalamin species.[9−11] Alternatively, enzymes utilizing AdoCbl catalyze radical-induced rearrangement reactions (isomerases; e.g., methylmalonyl Co-A mutase) or ribonucleotide reduction via Co−C bond homolysis to produce Co^{2+} cobalamin and an organic radical centered on the 5′-carbon of the Ado moiety.[8,12−16] This Ado• radical is capable of abstracting

† Present address: Department of Bacteriology, University of Wisconsin-Madison, Madison, WI 53706.

(1) Banerjee, R., Ed. *Chemistry and Biochemistry of B_{12}*; Wiley-Interscience: New York, 1999.
(2) Banerjee, R. *Biochemistry* **2001**, *40*, 6191−6198.
(3) Dolphin, D., Ed. *B_{12}*; Wiley: New York, 1982.
(4) Ludwig, M. L.; Drennan, C. L.; Matthews, R. G. *Structure* **1996**, *4*, 505−512.
(5) Ludwig, M. L.; Matthews, R. G. *Annu. Rev. Biochem.* **1997**, *66*, 269−313.
(6) Hodgkin, D. C. P.; Robertson, J. H.; Trueblood, K. N.; Prosen, R. J.; White, J. G. *Nature (London)* **1956**, *176*, 325.
(7) Finke, R. G.; Hay, B. P. *Inorg. Chem.* **1984**, *23*, 3041−3043.
(8) Banerjee, R. *Chem. Biol.* **1997**, *4*, 175−186.
(9) Matthews, R. G. *Acc. Chem. Res.* **2001**, *34*, 681−689.
(10) Drennan, C. L.; Huang, S.; Drummond, J. T.; Matthews, R. G.; Ludwig, M. L. *Science* **1994**, *266*, 1669−1674.
(11) Drennan, C. L.; Matthews, R. G.; Ludwig, M. L. *Curr. Opin. Struct. Biol.* **1994**, *4*, 919−929.
(12) Thoma, N. H.; Evans, P. R.; Leadlay, P. F. *Biochemistry* **2000**, *39*, 9213−9221.
(13) Thoma, N. H.; Leadlay, P. F. *Protein Sci.* **1996**, *5*, 1922−1927.
(14) Mancia, F.; Evans, P. R. *Struct. Fold. Des.* **1998**, *6*, 711−720.
(15) Gerfen, G. J.; Licht, S.; Willems, J.-P.; Hoffman, B. M.; Stubbe, J. *J. Am. Chem. Soc.* **1996**, *118*, 8192−8197.

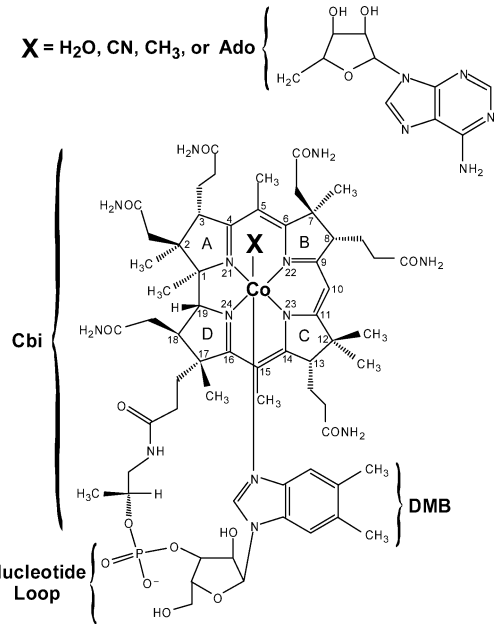

Figure 1. Chemical structure and numbering scheme for Co^{3+}Cbls, where **X** indicates the upper axial ligand.

a hydrogen atom from substrate as the first step in a protein-mediated substrate rearrangement reaction. Both MeCbl- and AdoCbl-dependent enzymes activate the organometallic Co−C bond to a spectacular degree; an increase by as much as 12 orders of magnitude has been reported for the rate of Co−C bond homolysis in isomerases.[17−20]

Despite extensive research on these unique cofactors, fundamental questions such as why nature has equipped cobalamins with a corrin macrocycle rather than a porphyrin ring, why cobalt is used rather than a more readily available metal center, and how the Co−C bond is activated by Cbl-dependent enzymes remain largely unanswered. The corrin macrocycle is significantly more complex than porphyrins, possessing lower symmetry and additional side chains that potentially allow for substantial interaction with protein active site residues.[10,21] The corrin π system contains 14 electrons distributed over 13 atoms (Figure 1),[22] as compared to 18 electrons distributed over 18 atoms that make up the porphyrin π system.[23] The more reduced nature of the corrin macrocycle as compared to that of porphyrins provides the former with considerably more conformational freedom. It has been postulated that Cbl-dependent enzymes take advantage of this increased flexibility to activate the Co−C bond through a butterfly bending motion of the corrin ring, as this would lead to steric crowding with the upper axial ligand.[2,19,24−27] However, numerous other mechanisms have been

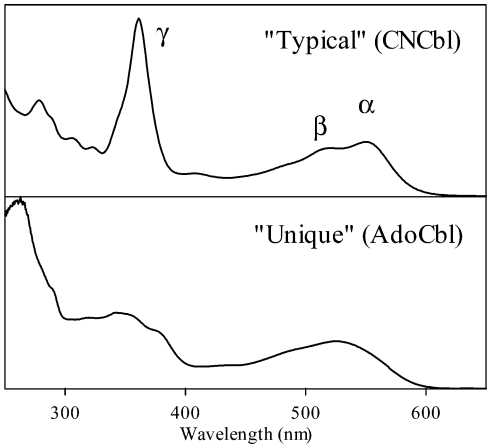

Figure 2. Room-temperature Abs spectra for aqueous solutions of CNCbl (top) and AdoCbl (bottom). Band designations are indicated in the "typical" CNCbl Abs spectrum.

proposed to contribute to this exalted activation of the Co−C bond for homolysis or heterolysis in B_{12}-dependent enzymes, for example, an electronic trans-effect involving the lower axial ligand,[19,27−29] corrin ring modulation through side chain interactions,[30,31] and protein-mediated conformational changes that involve the upper axial ligand, leading to Co−C bond tilting.[14,32] Electronic absorption (Abs) and circular dichroism (CD) spectroscopic techniques have been used extensively to probe changes in geometric and electronic properties of the cofactor upon protein binding,[31,33,34] but the lack of a suitable theoretical framework within which to interpret these data has greatly limited progress toward elucidation of Co−C bond activation mechanisms on the basis of spectroscopic data.

Most Cbl Abs spectra exhibit striking similarities between one another, as the corrin ligand is responsible for nearly all observed spectral features. While binding of cobalt to the metal-free corrin slightly perturbs the energies and relative intensities of the dominant absorption features, the overall shape of the spectrum is preserved.[22,35] Consequently, all observed electronic transitions for Co^{3+}Cbls have historically been assigned as being primarily $\pi \rightarrow \pi^*$ in character.[22,33,35] A "typical" Cbl Abs spectrum (Figure 2, top) is dominated by two features, the so-called α/β bands ($\epsilon \approx 8000-10\,000\ M^{-1}\ cm^{-1}$) in the visible spectral region and the γ band ($\epsilon \approx 25\,000\ M^{-1}\ cm^{-1}$) in the UV. It is widely accepted that the α/β bands arise from the same $\pi \rightarrow \pi^*$ transition, with the more intense α band being the electronic origin and the β band the first member of a progression in a vibrational mode involving primarily C═C stretches along the $C^5\cdots C^{15}$ vector of the corrin ring (Figure 1).[22,36] Several additional, considerably weaker features termed

(16) Magnusson, O. T.; Reed, G. H.; Frey, P. A. *Biochemistry* **2001**, *40*, 7773−7782.
(17) Brown, K. L.; Zou, X. *J. Inorg. Biochem.* **1999**, *77*, 185−195.
(18) Hay, B. P.; Finke, R. G. *J. Am. Chem. Soc.* **1986**, *108*, 4820−4829.
(19) Chowdhury, S.; Banerjee, R. *Biochemistry* **2000**, *39*, 7998−8006.
(20) Hay, B. P.; Finke, R. G. *J. Am. Chem. Soc.* **1987**, *109*, 8012−8018.
(21) Mancia, F.; Keep, N. H.; Nakagawa, A.; Leadlay, P. F.; McSweeney, S.; Rasmussen, B.; Bosecke, P.; Diat, O.; Evans, P. R. *Structure* **1996**, *4*, 339−350.
(22) Pratt, J. M. In *Chemistry and Biochemistry of B_{12}*; Banerjee, R., Ed.; Wiley: New York, 1999; pp 113−164.
(23) Makinen, M. W.; Churg, A. K. In *Iron Porphyrins*; Lever, A. B. P., Gray, H. B., Eds.; Addison-Wesley: Reading, MA, 1983; Vol. 1, pp 141−235.
(24) Chemaly, S. M.; Pratt, J. M. *J. Chem. Soc., Dalton Trans.* **1980**, 2274−2281.
(25) Glusker, J. P. In *B_{12}*; Dolphin, D., Ed.; Wiley: New York, 1982; Vol. 1, pp 23−106.
(26) Brown, K. L.; Brooks, H. B. *Inorg. Chem.* **1991**, *30*, 3420−3430.
(27) Jensen, K. P.; Sauer, S. P. A.; Liljefors, T.; Norrby, P. O. *Organometallics* **2001**, *20*, 550−556.
(28) Andruniow, T.; Zgierski, M. Z.; Kozlowski, P. M. *J. Phys. Chem. B* **2000**, *104*, 10921−10927.
(29) Pratt, J. M. In *Chemistry and Biochemistry of B_{12}*; Banerjee, R., Ed.; Wiley: New York, 1999; pp 73−112.
(30) Chowdhury, S.; Banerjee, R. *Biochemistry* **1999**, *38*, 15287−15294.
(31) Calafat, A. M.; Taoka, S.; Puckett, J. M.; Semerad, C.; Yan, H.; Luo, L. B.; Chen, H. L.; Banerjee, R.; Marzilli, L. G. *Biochemistry* **1995**, *34*, 14125−14130.
(32) Dong, S. L.; Padmakumar, R.; Banerjee, R.; Spiro, T. G. *J. Am. Chem. Soc.* **1999**, *121*, 7063−7070.
(33) Schneider, Z.; Stroinski, A. *Comprehensive B_{12}: Chemistry, Biochemistry, Nutrition, Ecology and Medicine*; De Gruyter: New York, 1987.
(34) Firth, R. A.; Hill, H. A. O.; Pratt, J. M.; Williams, R. J. P.; Jackson, W. R. *Biochemistry* **1967**, *6*, 2178−2189.
(35) Toohey, J. I. *Proc. Natl. Acad. Sci. U.S.A.* **1965**, *54*, 934.
(36) Salama, S.; Spiro, T. G. *J. Raman Spectrosc.* **1977**, *6*, 57−60.

D and E bands are sometimes observed between the α/β and γ bands, the origin of which remains controversial. Such "typical" Abs spectra are observed for nearly all cobalamin species, such as vitamin B_{12} (cyanocobalamin, CNCbl) and aquacobalamin (H_2OCbl^+), in which the upper axial position is occupied by cyanide and water molecules, respectively (Figure 1).[22,34]

In contrast, alkylcobalamins, such as MeCbl and AdoCbl, exhibit "unique" Abs spectra that differ from "typical" spectra in several ways (cf. Figure 2). While the α/β bands still appear to correspond to the electronic origin and a vibrational sideband associated with a single $\pi \rightarrow \pi^*$ transition, the β band is now considerably more intense than the α band. Moreover, the spacing between the β band and the prominent shoulder on its high-energy side, seemingly corresponding to the next member of the vibrational progression, exceeds the frequency of any corrin-based vibrational mode. Most striking, however, is that the intensity of the γ band is redistributed over several similarly intense transitions in the UV spectral region. The fact that the Co^{3+}Cbl absorption spectrum varies as a function of the upper axial ligand even though it is dominated by corrin $\pi \rightarrow \pi^*$ transitions suggests that extensive communication occurs between the axial ligands and the corrin macrocycle. As both B_{12} cofactors utilized by enzymatic systems exhibit "unique" Abs spectra, knowledge of the geometric and electronic factors distinguishing them from Cbl species exhibiting "typical" Abs spectra is of considerable interest; however, these factors are largely unexplored.

Significant advances in theoretical chemistry and computer technology have recently permitted high-level density functional theory (DFT) calculations to be performed on Cbl models that contain the actual corrin ring,[27,28,37−46] opening new avenues for investigations of structural and spectroscopic properties of Cbls. While most DFT studies reported to date were aimed at calculating structural parameters, Kozlowski and co-workers have used their computations to analyze the electronic Abs spectrum of CNCbl[47] and vibrational data of MeCbl.[48] The calculated Abs spectrum of a CNCbl model, obtained using the time-dependent DFT (TD-DFT) method in conjunction with the B3LYP hybrid functional, agrees well with the experimental spectrum after a uniform red-shift by ~0.5 eV. Reasonable agreement was also achieved between experimental and calculated Raman spectra of MeCbl, which permitted preliminary insight into the normal mode descriptions of corrin vibrations. Although these results demonstrate the tremendous potential of DFT for analyzing spectroscopic data of Cbls on the basis of computational predictions, a detailed correlation between spectroscopic and computational data has not yet been established, leaving a gap in the understanding of the electronic structures and, consequently, the reactivities of these exquisite cofactors.

In this paper, we present Abs, CD, magnetic CD (MCD), and resonance Raman (RR) spectroscopic data of a representative set of Co^{3+}Cbl species whose upper axial ligands span the spectrochemical series, including MeCbl, AdoCbl, CNCbl, and H_2OCbl^+. Also included to probe the effect of the lower axial ligand on the electronic properties of Cbls is 5′-deoxyadenosylcobinamide ($AdoCbi^+$), an AdoCbl derivative that lacks the nucleotide loop and instead binds a water molecule in the lower axial position (Figure 1). Spectroscopic data for each species are analyzed within the framework of TD-DFT to assign key electronic transitions and to generate experimentally validated electronic-structure descriptions. These studies permit detailed insight into the factors that distinguish Cbls exhibiting a "typical" Abs spectrum from those displaying a "unique" spectrum and provide a firm basis for future investigations aimed at elucidating the mechanisms of B_{12}-dependent enzymes.

2. Experimental Section

Chemicals/Cofactors. MeCbl, AdoCbl, CNCbl, and H_2OCbl^+ were purchased from Sigma and used as obtained. $AdoCbi^+$ was prepared enzymatically according to published procedures.[49−52] Specifically, $(CN)_2$Cbi was reduced to Co^{1+}Cbi using $NaBH_4$, and this reduced species served as the substrate for the ATP:cor(I)rinoid adenosyltransferase (CobA) from *Salmonella enterica* to generate $AdoCbi^+$. All Cbl species were dissolved in doubly distilled water at pH 7. H_2OCbl^+ solutions were subsequently adjusted to pH 5 using 0.1 M HCl (Sigma) to ensure complete conversion of hydroxycobalamin to H_2OCbl^+.[33]

Spectroscopy. Electronic Abs, CD, and MCD spectra were obtained using a Jasco J-715 spectropolarimeter in conjunction with an Oxford Instruments SM-4000 8T magnetocryostat. The samples used for low-temperature experiments were prepared in a 60% (v/v) glycerol glassing agent. Sample concentrations ranged from 0.15 to 0.8 mM and were determined spectrophotometrically at 300 K on the basis of published molar extinction coefficients.[1,33,34] All MCD spectra reported in this paper were obtained by subtracting the −7 T spectrum from the +7 T spectrum to eliminate contributions from the natural CD.

RR spectra were obtained upon excitation with a Coherent I-305 Ar^+ ion laser either directly (between 351 and 514 nm) or in conjunction with a Coherent 599-01 dye circulator (570−615 nm) with 10−50 mW laser power at the sample. The scattered light was collected using a ~135° backscattering arrangement, dispersed by an Acton Research triple monochromator (equipped with 300, 1200, and 2400 grooves/mm gratings), and analyzed with a Princeton Instruments Spec X: 100BR deep depletion, back-thinned CCD camera. All samples (prepared as described above except that glycerol was omitted in this case) were frozen in NMR tubes and placed in an EPR dewar filled with liquid N_2 to prevent photolysis during data collection.[53] For AdoCbl and MeCbl, RR data were also collected on frozen pellets situated directly in the EPR dewar to eliminate the broad background signal near 450 cm^{-1} arising from the NMR tube, which partially overlaps

(37) Andruniow, T.; Zgierski, M. Z.; Kozlowski, P. M. *Chem. Phys. Lett.* **2000**, *331*, 502−508.
(38) Andruniow, T.; Zgierski, M. Z.; Kozlowski, P. M. *Chem. Phys. Lett.* **2000**, *331*, 509−512.
(39) Andruniow, T.; Zgierski, M. Z.; Kozlowski, P. M. *J. Am. Chem. Soc.* **2001**, *123*, 2679−2680.
(40) Kozlowski, P. M. *Curr. Opin. Chem. Biol.* **2001**, *5*, 736−743.
(41) Torrent, M.; Musaev, D. G.; Morokuma, K.; Ke, S.-C.; Warncke, K. *J. Phys. Chem. B* **1999**, *103*, 8618−8627.
(42) Randaccio, L.; Geremia, S.; Nardin, G.; Slouf, M.; Srnova, I. *Inorg. Chem.* **1999**, *38*, 4087−4092.
(43) Marques, H. M.; Zou, X.; Brown, K. L. *J. Mol. Struct.* **2000**, *520*, 75−95.
(44) Marques, H. M.; Brown, K. L. *Coord. Chem. Rev.* **2002**, *225*, 123−158.
(45) Brown, K. L.; Marques, H. M. *J. Inorg. Biochem.* **2001**, *83*, 121−132.
(46) Sirovatka, J. M.; Rappe, A. K.; Finke, R. G. *Inorg. Chim. Acta* **2000**, *300−302*, 545−555.
(47) Andruniow, T.; Kozlowski, P. M.; Zgierski, M. Z. *J. Chem. Phys.* **2001**, *115*, 7522−7533.
(48) Andruniow, T.; Zgierski, M. Z.; Kozlowski, P. M. *J. Phys. Chem. A* **2002**, *106*, 1365−1373.
(49) Suh, S.-J.; Escalante-Semerena, J. C. *J. Bacteriol.* **1995**, *177*, 921−925.
(50) Fonseca, M. V.; Escalante-Semerena, J. C. *J. Bacteriol.* **2000**, *182*, 4304−4309.
(51) Fonseca, M. V.; Buan, N. R.; Horswill, A. R.; Rayment, I.; Escalante-Semerena, J. C. *J. Biol. Chem.* **2002**, *277*, 33127−33131.
(52) Fonseca, M. V.; Escalante-Semerena, J. C. *J. Biol. Chem.* **2001**, *276*, 32101−32108.
(53) Note that previously published RR spectra of Co^{2+}Cbl (see: Salama, S.; Spiro, T. G. *J. Raman Spectrosc.* **1977**, *6*, 57−60) indicate that a single feature at ~1500 cm^{-1} could potentially interfere with RR excitation profile experiments for Co^{3+}Cbls. However, as the maximum enhancement of this feature occurs for excitation at 474 nm, possible contributions from traces of Co^{2+}Cbl to our RR spectra obtained with 514.5 nm excitation are negligible.

with the Co−C stretch. RR excitation profiles were obtained by quantifying the peak intensities relative to the ice peak at 228 cm^{-1} or an internal standard of 100 μM K_2SO_4 (for MeCbl pellet). All RR excitation profiles shown in this study represent the average of at least three independent data sets.

Computational Models. Approximate models of MeCbl, CNCbl, and H_2OCbl^+ were generated starting from the corresponding highest-resolution X-ray data reported to date.[54−56] The DMB base was either maintained or modeled as an imidazole, where the Co−N bond length and relative orientation of the five-membered ring of the base were preserved, or as an amine, and the entire nucleotide loop was replaced by an H atom at C^{17} (see Figure 1).[57] All other corrin ring substituents were replaced by H atoms separated by 1 Å from the neighboring C atoms.[58] TD-DFT calculations were also performed on analogous MeCbl models obtained by (i) a full geometry optimization of all atoms and (ii) an optimization of only the upper and lower-axial ligands (all other atoms were kept at reported X-ray structure coordinates). As expected, the fully optimized model showed some flattening of the corrin ring (from a fold angle of 14.7° to 4.7°) due to relaxation of steric constraints formally imposed by the DMB, while the partially optimized model exhibited a minor increase in Co−C and Co−N_{ax} bond lengths. However, both of these additional models showed TD-DFT results very similar to those obtained using the crystal structure coordinates. Thus, for all subsequent calculations, models based on published crystal structures were used as these represent the best replica of the entire corrinoid species. Because structural data for cobinamides are not yet available, a model of $MeCbi^+$ was generated on the basis of the approximate MeCbl structure described above but with a water molecule replacing the axial base. The positions of both axial ligands were optimized by DFT energy minimization using the Amsterdam Density Functional (ADF) 2000.02 suite of programs,[59,60] while all other atoms were kept frozen. The optimization was carried out on a home-built cluster of eight Pentium III processors using ADF basis set II, an integration constant of 3.0, and the Vosko−Wilk−Nusair local density approximation (VWN-LDA)[61] with the nonlocal gradient corrections of Becke for exchange[62] and Perdew for correlation.[63] Core orbitals were frozen through 1s (O, N, C) and 3p (Co). Coordinates of all Cbl and Cbi models discussed in the text are included in the Supporting Information (Tables S1−S4).

Single-Point DFT Calculations. Single-point DFT calculations were performed using the ORCA 2.0 software package developed by Dr. Frank Neese (MPI Mülheim, Germany).[64] A series of basis sets and functionals were employed on all three models of each Cbl studied that differed with respect to the lower axial ligand (vide supra). The Perdew−Wang LDA (PW-LDA)[65] with the gradient corrections by Becke[62] and Perdew[63] were employed together with the following basis sets: (i) TZVP (Ahlrichs polarized triple-ζ valence) basis[66,67] in conjunction with the TZV/J auxiliary basis,[68] (ii) DGauss (Gaussian polarized double-ζ valence orbital) basis[69] along with the Demon/J auxiliary basis,[69] and (iii) same as (ii) but with the TZVP basis[66,67] for Co. Becke's three-parameter hybrid functional for exchange[70,71] combined with the Lee−Yang−Parr correlation functional[72] (B3LYP/G) using the default 20% Hartree−Fock exchange were employed together with (iv) the SV(P) (Ahlrichs polarized split valence) basis[67,73] in conjunction with the SV/C auxiliary basis[68] and (v) same as (iv) but with the TZVP basis[66,67] for Co. The size of the integration grid used in all cases was 3 (Lebedev 194 points). Isosurface plots of molecular orbitals were generated with the gOpenMol program developed by Laaksonen[74,75] using an isodensity value of 0.03 b^{-3}.

TD-DFT Calculations. Vertical excitation energies and transition dipole moments for all Cbl and Cbi models were calculated by the TD-DFT method[76−78] within the Tamm−Dancoff approximation (TDA)[79,80] employing both the gradient corrected and the hybrid functionals and all basis sets described above. Convergence of the TD-DFT calculation required use of the resolution of the identity approximation (RI) in calculating the Coulomb term.[81] In each case, 40 excited states were calculated by including all one-electron excitations within an energy window of ±3 hartrees with respect to the HOMO/LUMO energies. All TD-DFT calculations were performed using the ORCA 2.0 package.

Abs and RR Excitation Profile Data Analysis. Abs and RR excitation profile data were iteratively fit using the time-dependent theory of electronic spectroscopy developed by Heller,[82] as implemented in a Mathcad 8.0 script.[83] A direct modeling approach[84] was used to determine the set of excited-state parameters that yields the best agreement between simulated and experimental Abs band shape and RR excitation profile data.

3. Results and Analysis

3.1. Spectroscopic Data. (i) Abs, CD, and MCD. Figure 3 shows electronic absorption (Abs), circular dichroism (CD), and magnetic CD (MCD) spectra of three different cobalamin species, including methylcobalamin (MeCbl), aquacobalamin (H_2OCbl^+), and vitamin B_{12} (cyanocobalamin, CNCbl). Comparison of these three sets of spectra reveals the effect of the *upper* axial ligand on the electronic structures of Cbls. These ligands were chosen to span a wide range of the spectrochemical series, with 10 Dq increasing in the order H_2O (weak σ- and π-donor) < Me^- (strong σ-donor) < CN^- (moderate σ-donor, strong π-acceptor). Consistent with the diamagnetic ground state of Co^{3+}-cobalamins, all features in the MCD spectra of Figure 3 were found to be temperature independent.

H_2OCbl^+. The Abs spectrum of H_2OCbl^+ (Figure 3B, top) shows the three sets of bands that characterize a "typical" cobalamin spectrum: the α/β bands previously assigned to the

(54) Randaccio, L.; Furlan, M.; Geremia, S.; Slouf, M.; Srnova, I.; Toffoli, D. *Inorg. Chem.* **2000**, *39*, 3403−3413.
(55) Bouquiere, J. P.; Finney, J. L.; Lehmann, M. S.; Lindley, P. F.; Savage, H. F. J. *Acta Crystallogr., Sect. B−Struct. Commun.* **1993**, *49*, 79−89.
(56) Kratky, C.; Farber, G.; Gruber, K.; Wilson, K.; Dauter, Z.; Nolting, H. F.; Konrat, R.; Kräutler, B. *J. Am. Chem. Soc.* **1995**, *117*, 4654−4670.
(57) The structural parameters of the imidazole modeling the DMB base were obtained from a full geometry optimization of the H_2OCbl^+ model.
(58) TD-DFT calculations on a similar MeCbl model using more typical C−H bond lengths of 1.08 Å were performed, and results showed no significant differences in MO composition or transition state energies as compared to the results from the model with shorter C−H bond lengths.
(59) Baerends, E. J.; Ellis, D. E.; Ros, P. *Chem. Phys.* **1973**, *2*, 41−51.
(60) te Velde, G.; Baerends, E. J. *J. Comput. Phys.* **1992**, *99*, 84−98.
(61) Vosko, S. H.; Wilk, L.; Nusair, M. *Can. J. Phys.* **1980**, *58*, 1200−1211.
(62) Becke, A. D. *J. Chem. Phys.* **1988**, *84*, 4524−4529.
(63) Perdew, J. P. *Phys. Rev. B* **1986**, *33*, 8822−8824.
(64) Neese, F.; Solomon, E. I. *Inorg. Chem.* **1999**, *38*, 1847−1865.
(65) Perdew, J. P.; Wang, Y. *Phys. Rev. B* **1992**, *45*, 13244−13249.
(66) Schäfer, A.; Horn, H.; Ahlrichs, R. *J. Chem. Phys.* **1994**, *100*, 5829−5835.
(67) Ahlrichs, R., unpublished results.
(68) The Ahlrichs auxiliary basis sets were obtained from the TurboMole basis set library under ftp.chemie.uni-karlsruhe.de/pub/cbasen. Weigend, F.; Haeser, M. *Theor. Chem. Acc.* **1997**, *97*, 331−340.
(69) Godbout, N.; Salahub, D. R.; Andzeim, J.; Wimmer, E. *Can. J. Chem.* **1992**, *70*, 560.
(70) Becke, A. D. *J. Chem. Phys.* **1993**, *98*, 1372−1377.
(71) Becke, A. D. *J. Chem. Phys.* **1993**, *98*, 5648−5652.
(72) Lee, C.; Yang, W.; Parr, R. G. *Phys. Rev. B* **1988**, *37*, 785−789.
(73) Schäfer, A.; Horn, H.; Ahlrichs, R. *J. Chem. Phys.* **1992**, *97*, 2571−2577.
(74) Laaksonen, L. *J. Mol. Graphics* **1992**, *10*, 33.
(75) Bergman, D. L.; Laaksonen, L.; Laaksonen, A. *J. Mol. Graphics Modell.* **1997**, *15*.
(76) Bauernschmitt, R.; Ahlrichs, R. *Chem. Phys. Lett.* **1996**, *256*, 454−464.
(77) Casida, E. M.; Jamorski, C.; Casida, K. C.; Salahub, D. R. *J. Chem. Phys.* **1998**, *108*, 4439−4449.
(78) Stratman, R. E.; Scuseria, G. E.; Frisch, M. J. *J. Chem. Phys.* **1998**, *109*, 8218−8224.
(79) Hirata, S.; Head-Gordon, M. *Chem. Phys. Lett.* **1999**, *302*, 375−382.
(80) Hirata, S.; Head-Gordon, M. *Chem. Phys. Lett.* **1999**, *314*, 291−299.
(81) Neese, F.; Olbrich, G. *Chem. Phys. Lett.* **2002**, 170−178.
(82) Tannor, D. T.; Heller, E. J. *J. Chem. Phys.* **1982**, *77*, 202−218.
(83) Brunold, T. C.; Tamura, N.; Kitajima, N.; Moro-oka, Y.; Solomon, E. I. *J. Am. Chem. Soc.* **1998**, *120*, 5674−5690.
(84) Myers, A. B.; Mathies, R. A. *Biological Application of Raman Spectroscopy*; Wiley: New York, 1987; Vol. 2.

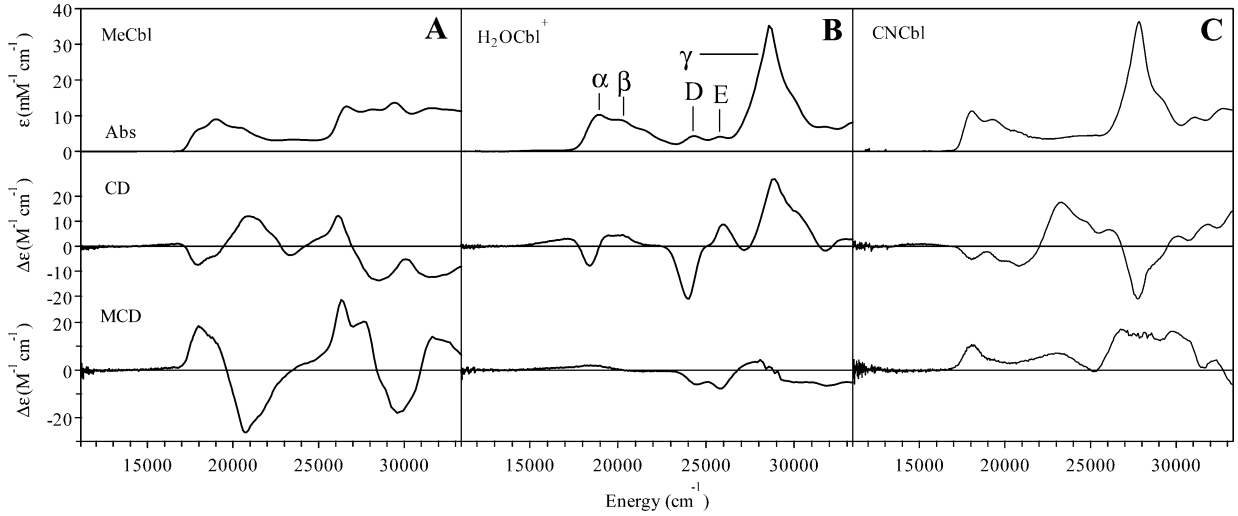

Figure 3. Absorption (top), CD (center), and 7 T MCD (bottom) spectra recorded at 4.5 K of MeCbl (A), H_2OCbl^+ (B), and CNCbl (C). Band designations are given for H_2OCbl^+.

corrin-based HOMO → LUMO (i.e., $\pi \rightarrow \pi^*$) transition polarized along the long axis of the corrin macrocycle ($C^5 \cdots C^{15}$ vector, Figure 1);[22,36] the D/E bands for which definitive assignment has been lacking;[22] and the γ band attributed to a corrin $\pi \rightarrow \pi^*$ transition polarized along the short corrin axis ($Co \cdots C^{10}$ vector, Figure 1).[36,85] The α/β bands centered at ~18 840/20 110 cm^{-1} along with the poorly resolved adjacent features at higher energy have previously been assigned to members of a vibrational progression in a corrin mode, ν_{LA}, primarily involving stretches of the long-axis C=C double bonds oriented along the $C^5 \cdots C^{15}$ vector (Figure 1).[22,36] The frequency of this mode in the electronic ground state is 1496 cm^{-1}, indicating a reduction by ~9% (i.e., to 1270 cm^{-1}, estimated from the spacing between the α and β bands) in the electronic excited state. This decrease in frequency of ν_{LA} is consistent with the expected weakening of the C=C bonds upon corrin $\pi \rightarrow \pi^*$ excitation due to the decrease in π-bonding and increase in π-antibonding character on the macrocycle. The α/β region of the H_2OCbl^+ CD spectrum (Figure 3B, center) exhibits one band of large negative intensity that coincides with the α band in the Abs spectrum and several weak features of positive intensity, one of which occurs at lower energy than the α band. The α/β region of the MCD spectrum (Figure 3B, bottom) shows only one weak, temperature-independent *B*-term feature that coincides with the α band.

The D/E bands of H_2OCbl^+ are quite well resolved in the Abs spectrum (Figure 3B, top), yet two other features of relatively high intensity appear to dominate the CD spectrum in this region (Figure 3B, center). In the MCD spectrum, two negative features are present in the D/E region (Figure 3B, bottom) that correspond precisely with the D/E bands observed in the Abs spectrum. Thus, our data indicate that at least four different electronic transitions contribute to the D/E region of the H_2OCbl^+ spectra.

The γ region of the H_2OCbl^+ spectra (Figure 3B) is composed of at least two overlapping bands, as evidenced by the shoulder on the high-energy side of the most intense Abs feature and the presence of two positive CD features in this region. The fact that these two features are oppositely signed in the corresponding MCD spectrum (Figure 3B, bottom) reveals that they cannot be vibronic components of a single transition but instead arise from two distinct electronic transitions.

CNCbl. The Abs, CD, and MCD spectra of CNCbl (Figure 3C) exhibit the same basic features as those of H_2OCbl^+ (Figure 3B), however, with several subtle differences. The α band is red-shifted by 760 cm^{-1} to 18 080 cm^{-1}, and the spacing between adjacent members of the vibrational progression increases slightly to ~1300 cm^{-1}. Moreover, there is no indication for the presence of a low-energy feature similar to the one observed in the H_2OCbl^+ CD spectrum (cf. Figure 3B and 3C, center). While the D/E bands are unresolved in the CNCbl Abs spectrum, at least two features can be discerned in this region of the corresponding CD and MCD spectra. The γ region again reveals the presence of at least two electronic transitions, giving rise to the very intense Abs band with a well-developed shoulder on its high-energy side, which is red-shifted by 880 cm^{-1} with respect to the γ band in the H_2OCbl^+ spectra (cf. Figure 3B and 3C).

MeCbl. The dominant features in the "unique" Abs spectrum of MeCbl (Figure 3A, top) can be classified in a manner similar to those observed in a "typical" Cbl Abs spectrum; however, key differences exist that allow for experimental insight into the effects of the upper axial ligand on the corrinoid electronic structure. While the α/β bands again appear to correspond to the electronic origin and the first member of a progression in ν_{LA} associated with a single $\pi \rightarrow \pi^*$ transition, the fact that the β band is now more intense than the α band (suggesting a Huang−Rhys parameter $S(\nu_{LA}) > 1$) appears to indicate that distortions in the corresponding excited state relative to the ground-state equilibrium geometry are considerably greater in this case than for H_2OCbl^+ and CNCbl (where $S(\nu_{LA}) < 1$). Importantly, the presence of the derivative-shaped features in the α/β regions of the MeCbl CD and MCD spectra (Figure 3A, center and bottom) suggests that the prominent shoulder on the high-energy side of the β band in the MeCbl Abs spectrum (Figure 3A, top), previously ascribed to the second member of the progression in ν_{LA},[22] actually corresponds to the origin of another electronic transition in this region. Hence, the

(85) Classification of other features in the "typical" Abs spectra of Cbls exists (see, for example: Pratt, J. M. In *Chemistry and Biochemistry of B_{12}*; Banerjee, R., Ed.; Wiley: New York, 1999), but analysis of the corresponding transitions is beyond the scope of this study.

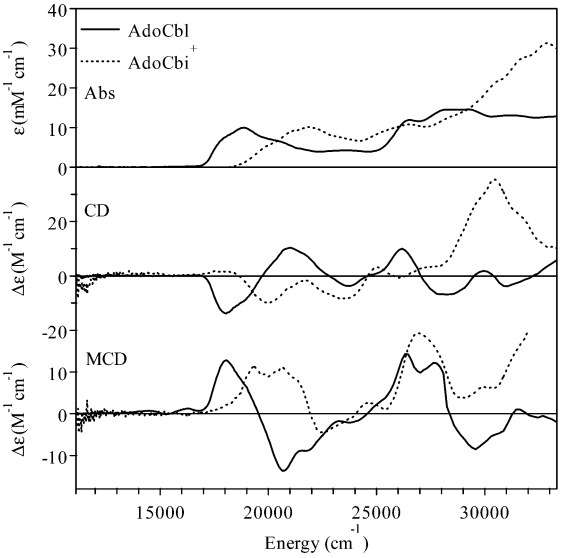

Figure 4. Comparison of 4.5 K Abs (top), CD (center), and 7 T MCD (bottom) spectra of AdoCbl and $AdoCbi^+$.

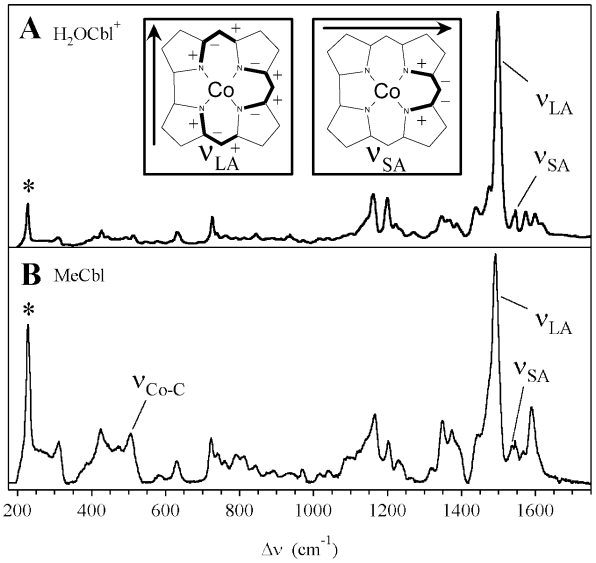

Figure 5. RR spectra at 77 K of H_2OCbl^+ (top) and MeCbl (bottom) obtained with 514.5-nm excitation. Insets: Normal mode descriptions of ν_{LA} (left) and ν_{SA} (right), adapted from ref 48.

α/β region of the MeCbl Abs spectrum differs from that of "typical" cobalamin spectra in two significant ways: (i) the β band gains intensity relative to the α band, and (ii) a second relatively intense electronic transition contributes to the Abs spectrum. Alternatively, the D/E region of the MeCbl spectra, which is composed of at least two electronic transitions as revealed by the partially resolved CD and MCD spectra in this region, is reminiscent of "typical" Cbl spectra.

The most unique aspect of the MeCbl Abs spectrum is that the intensity of the γ band is redistributed over three partially resolved features in the UV region that carry similar intensities. As these features are separated by $\sim$1500 cm^{-1}, which is significantly larger than the frequency of ν_{LA} in the lowest-energy $\pi \rightarrow \pi^*$ excited state corresponding to the α/β bands (vide supra), and are oppositely signed in the CD and/or MCD spectra, they are assigned to at least three distinct electronic transitions rather than a vibrational progression associated with a single transition. Thus, the number of electronic transitions in the γ region, similar to the α/β region discussed above, also increases from the "typical" to "unique" Cbl spectra.

AdoCbl and $AdoCbi^+$. Figure 4 compares the Abs, CD, and MCD spectra of AdoCbl and its derivative 5′-deoxyadenosylcobinamide ($AdoCbi^+$) that lacks the nucleotide loop and the pendant DMB group and instead binds a water molecule in the lower axial position[30] (Figure 1). Consistent with the diamagnetic ground state of low spin Co^{3+} in AdoCbl and $AdoCbi^+$, all features in the MCD spectrum of this species are also temperature independent. Remarkably, despite the fact that the combination of Abs, CD, and MCD spectroscopies offers a highly sensitive probe of electronic excited states, all three spectra of AdoCbl are nearly identical to those of MeCbl (Figure 3A). This result indicates that the steric repulsion between the Ado moiety and the corrin ring, which partially compensates for the steric interaction between the macrocycle and the DMB group and thus leads to a substantially flatter corrin conformation in AdoCbl than in MeCbl,[86] has negligible effects on the cofactor electronic structure. Consequently, the marked changes in the electronic spectra associated with substitution of the upper (Figure 3) and lower (Figure 4) axial ligands are primarily electronic and not steric in nature.

Comparison of the two sets of spectra in Figure 4 reveals the effect of the *lower* axial ligand on the electronic structures of Cbl species. Consequently, the large differences between the AdoCbl and $AdoCbi^+$ spectra suggest that the lower axial ligand is similarly as important as the upper axial ligand in modulating the electronic properties of Cbls. The onset to the lowest energy Abs feature of $AdoCbi^+$ is blue-shifted by $\sim$2000 cm^{-1} as compared to the onset of the α band of AdoCbl, suggesting that the HOMO/LUMO gap increases substantially upon substitution of the DMB ligand by a water molecule. However, no other correlations can be made without the aid of computations between the dominant features in the $AdoCbi^+$ spectra and those in the "typical" and "unique" Cbl spectra presented in Figure 3.

In summary, our data presented in Figures 3 and 4 demonstrate that the axial ligands have a profound influence on the electronic structure of Cbls. A direct correlation between the σ-donor strength of the axial ligands and the position of the lowest-energy Abs feature (the α/β bands) is observed, with the stronger donors causing a significant red-shift of the corresponding transition. Provided that previous assignments of the dominant features in the electronic spectra of corrinoids as corrin $\pi \rightarrow \pi^*$ transitions[22] are correct, these results suggest that a mechanism exists by which the axial ligands modulate the electronic properties of the corrin macrocycle. Exploration of this mechanism along with band assignments for the corrinoid spectra in Figures 3 and 4 are presented in the Spectral Assignments section below.

(ii) RR Data. Figure 5 shows resonance Raman (RR) spectra of H_2OCbl^+ and MeCbl obtained with 514.5 nm (19 436 cm^{-1}) laser excitation. Despite the fact that the two species exhibit markedly different electronic Abs, CD, and MCD spectra (Figure 3), their RR spectra are strikingly similar. In both cases, the dominant features are due primarily to corrin vibrations (Table 1), with the most intense band at $\sim$1500 cm^{-1} corre-

(86) The fold angle ϕ is described by the angle between the planes formed by N21−C4−C5−C6−N22−C9−C10 and C10−C11−N23−C14−C15−C16−N24. For AdoCbl, ϕ is 13.3° (see ref 55), and for MeCbl, ϕ is 14.7° (see ref 54).

Table 1. Frequencies of Selected Corrinoid Vibrational Modes Obtained Using RR Spectroscopy

corrinoid	ν_{Co-C} (cm^{-1})	ν_{LA} (cm^{-1})	ν_{SA} (cm^{-1})
H_2OCbl^+[a]		1499	1543
CNCbl		1497	1542
MeCbl	505	1490	1542
AdoCbl	424	1493	1540
$AdoCbi^+$	423	1492	1534

[a] Taken at pH 5.

sponding to the long-axis polarized corrin mode ν_{LA} depicted schematically in the inset of Figure 5. This similarity indicates that substitution of the water ligand in H_2OCbl^+ by the methyl group in MeCbl does not drastically alter intracorrin bonding. Intriguingly, however, the 514.5-nm excited RR spectrum of MeCbl exhibits an additional band of significant intensity at 505 cm^{-1}, previously assigned by Spiro and co-workers[87,88] to the Co−C stretching mode ν_{Co-C} on the basis of isotopic labeling experiments. Enhancement of this mode upon excitation in resonance with a corrin-based $\pi \rightarrow \pi^*$ transition provides further evidence that the π system of the corrin macrocycle is electronically coupled to the Co−C bond, possibly implying that enzymatic Co−C bond activation may involve corrin ring deformation (vide infra).

RR Excitation Profiles. Although RR spectroscopy alone does not aid significantly in evaluating contributions of the axial ligands to the electronic structures of corrinoids, this technique is extremely well suited to resolve overlapping Abs bands and to obtain information regarding the polarizations of key electronic transitions. It has previously been shown that corrin-based $\pi \rightarrow \pi^*$ transitions that are polarized along the $C^5 \cdots C^{15}$ vector (Figure 1) give rise to almost exclusive enhancement of ν_{LA}, whereas those polarized along the $Co \cdots C^{10}$ vector predominantly enhance a corrin mode peaking at ~1540 cm^{-1} that primarily involves the short-axis C=C stretches (ν_{SA}, see inset in Figure 5).[48] The relative intensities of these two corrin modes, along with ν_{Co-C} in the case of MeCbl, were monitored as a function of excitation wavelength to obtain the RR excitation profiles shown in Figure 6.

The RR excitation profile data for H_2OCbl^+ (Figure 6A) reveal that a single electronic transition polarized along the $C^5 \cdots C^{15}$ vector dominates the α/β region of the Abs spectrum, consistent with the spectral analysis presented above. Alternatively, for MeCbl, the presence of two distinct electronic transitions in the α/β region, as revealed by our MCD data (Figure 3), can also be inferred from the RR excitation profiles (Figure 6B). The first transition peaks at ~17 800 cm^{-1} and primarily enhances ν_{Co-C} and ν_{LA}, whereas the second transition is centered near 21 000 cm^{-1} and predominantly enhances ν_{LA} and, to some extent, ν_{SA}. The fact that ν_{SA} is only enhanced for excitation in resonance with the higher-energy transition indicates that the two transitions possess slightly different polarizations.

RR excitation profile data were also obtained in the UV to gain polarization information on the dominant transitions in the γ region of the "typical" and "unique" Cbl Abs spectra. The

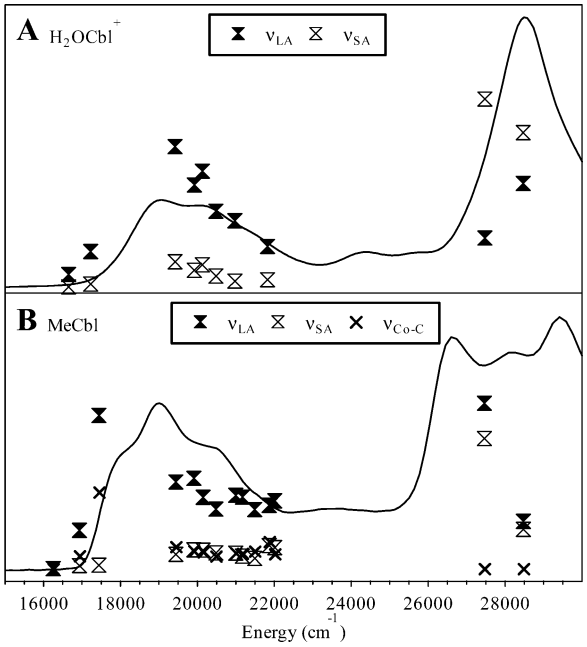

Figure 6. 4.5 K Abs spectra and 77 K RR excitation profile data for H_2OCbl^+ (top) and MeCbl (bottom).

RR spectra of H_2OCbl^+ obtained with 364 and 351 nm (27 473 and 28 490 cm^{-1}) laser excitation show greater enhancement of ν_{SA} than ν_{LA}, indicating that the dominant transition in the γ region (Figure 3B) is primarily short-axis polarized. The increase in intensity of ν_{LA} relative to ν_{SA} on approaching the Abs shoulder at ~30 000 cm^{-1} suggests that the transition responsible for this feature has a large long-axis polarized component. In the case of MeCbl, UV excitation also significantly enhances ν_{SA}, but the relative intensity of ν_{LA} is considerably larger than that for H_2OCbl^+. The fact that the intensity ratio of ν_{SA} and ν_{LA} varies as a function of excitation wavelength indicates that the intense transitions in the γ region of the MeCbl Abs spectrum have distinct polarizations, possessing varying degrees of short-axis and long-axis polarized components.

3.2. Spectral Analysis. In this section, a quantitative analysis of the spectroscopic data presented above is performed to establish a rigorous testing ground for the calculated electronic descriptions discussed in the subsequent section.

(i) Gaussian Deconvolutions. The Abs, CD, and MCD data presented in Figures 3 and 4 were iteratively fit with the fewest possible number of Gaussian bands to resolve the major electronic transitions contributing to the Abs spectrum of each corrinoid species included in this study. Band positions and bandwidths were initially chosen to best fit the MCD spectrum (as it was most well-resolved) and then adjusted iteratively to achieve optimal agreement with all three spectra for each species. The results obtained from Gaussian deconvolutions of the spectra of H_2OCbl^+, a representative example of a Cbl species exhibiting a "typical" Abs spectrum, and MeCbl, representative of a Cbl species displaying a "unique" Abs spectrum, are shown in Figure 7, and the corresponding fitting parameters are listed in Table 2. Results from iterative fits of the Abs, CD, and MCD spectra of CNCbl, AdoCbl, and $AdoCbi^+$ (Figures 3 and 4) are included in the Supporting Information (Tables S6, S7, and S9 and Figures S1−S3).

H_2OCbl^+. As anticipated on the basis of the qualitative spectral analysis presented in the previous section, Gaussian

(87) Dong, S. L.; Padmakumar, R.; Banerjee, R.; Spiro, T. G. *J. Am. Chem. Soc.* **1996**, *118*, 9182−9183.
(88) Dong, S. L.; Padmakumar, R.; Banerjee, R.; Spiro, T. G. *Inorg. Chim. Acta* **1998**, *270*, 392−398.

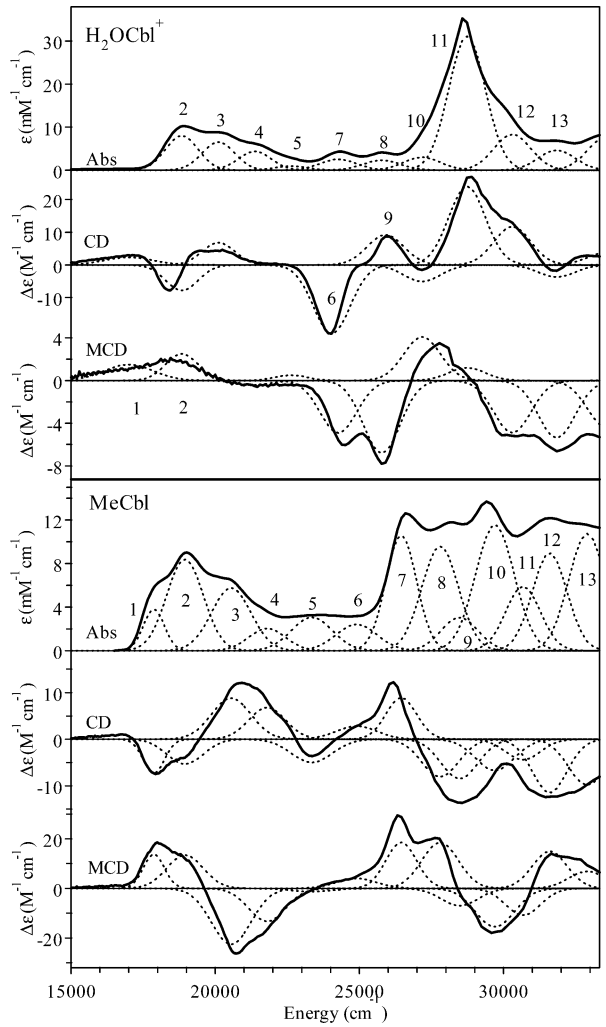

Figure 7. Solid lines: 4.5 K Abs, CD, and 7 T MCD spectra of H_2OCbl^+ (top three panels) and MeCbl (bottom three panels). Dotted lines: Gaussian deconvolutions of the experimental spectra. Note that bands 1, 6, and 9 observed in the CD and MCD spectra of H_2OCbl^+ do not appreciably contribute to the Abs spectrum. The fit parameters are given in Table 2.

deconvolution of the H_2OCbl^+ spectra (Figure 7, top) confirms that the α/β region of the Abs spectrum is dominated by a single electronic transition. The four equally spaced Gaussians used to model the Abs envelope in this region are members of a vibrational progression in a mode of $\sim$1250 cm^{-1}, identified as ν_{LA} on the basis of the RR data presented in Figures 5 and 6. Notably, the weak feature observed in the CD spectrum (band 1) that appears lower in energy than the α band has no obvious counterpart in the Abs spectrum, suggesting that the corresponding transition is predominantly magnetic dipole in character and thus presumably involves an MO possessing significant Co^{3+} 3d orbital character. As the α band has traditionally been referred to as the electronic origin of the corrin-based HOMO $\rightarrow$ LUMO ($\pi \rightarrow \pi^*$) transition,[22] this result implies that in H_2OCbl^+ an MO with significant Co 3d orbital character (hence the large magnetic dipole intensity) is in close energetic proximity to the HOMO/LUMO of the free corrin macrocycle.

Gaussian deconvolution of the H_2OCbl^+ spectra reveals further that two distinct electronic transitions are responsible for the D/E bands in the corresponding Abs spectra, as the spacing between the two bands of $\sim$1500 cm^{-1} (bands 8 and 9 in Table 2) exceeds the frequency of the corrin-based vibrational

Table 2. Fit Parameters from Gaussian Deconvolutions of the Abs, CD, and MCD Spectra of H_2OCbl^+ and MeCbl (Figure 7, Top and Bottom, Respectively)

corrinoid	band	energy (cm^{-1})	ϵ (Abs) ($M^{-1}\,cm^{-1}$)	$\Delta\epsilon$ (CD) ($M^{-1}\,cm^{-1}$)	$\Delta\epsilon$ (MCD) ($M^{-1}\,cm^{-1}$)
H_2OCbl^+	1	17 000	0	2.3	1.5
	2	18 840	8000	−7.8	2.5
	3	20 110	6540	6.8	0.0
	4	21 370	4375	0.0	−0.4
	5	22 625	920	0.0	0.5
	6	24 040	0	−21.0	0.0
	7	24 270	2515	0.0	−4.9
	8	25 775	2300	0.0	−6.8
	9	25 905	0	9.2	0.0
	10	27 175	3000	−5.1	4.1
	11	28 735	31125	24.1	1.2
	12	30 305	8345	11.8	−4.9
	13	31 845	4645	−3.7	−5.4
	14	33 555	7700	3.8	−4.4
MeCbl	1	17 870	3770	−7.3	13.7
	2	18 950	8365	−5.3	13.4
	3	20 550	5740	8.8	−22.5
	4	21 800	2030	6.8	−13.3
	5	23 350	3060	−5.0	−1.3
	6	24 900	2420	2.8	4.0
	7	26 450	10610	8.9	23.4
	8	27 800	9600	−8.1	18.6
	9	28 475	3060	−8.5	−7.0
	10	29 700	11540	−6.7	−15.6
	11	30 675	5910	−4.4	−10.8
	12	31 600	8970	−11.5	15.0
	13	32 900	10770	−9.9	6.9

modes ν_{LA} and ν_{SA} along which the dominant excited-state distortions occur (vide supra). Two additional electronic transitions are readily identified in this region, giving rise to the prominent derivative-shaped CD feature centered at $\sim$25 000 cm^{-1}. However, these transitions do not noticeably contribute to the corresponding Abs spectrum, suggesting that they are primarily magnetic dipole in character.

The γ region of the H_2OCbl^+ Abs spectrum is well reproduced by a single intense band, assigned to a short-axis polarized corrin $\pi \rightarrow \pi^*$ transition on the basis of the RR excitation profile data (Figure 6A), that is accompanied on either side by a considerably weaker feature. The irregular spacings and relative intensities indicate that these three features contributing to the γ region of the Abs spectrum correspond to three different electronic transitions rather than vibrational sidebands associated with a single electronic transition.

CNCbl. Spectral deconvolution of the CNCbl data, the other species included in this study that exhibits a "typical" Cbl Abs spectrum (Figure 3C), yielded very similar results. However, an interesting difference between H_2OCbl^+ and CNCbl is that the low-energy feature observed in the CD spectrum of the former species (band 1 in Figure 7, top) is not present in the spectra of the latter.

MeCbl. Iterative fitting of the Abs, CD, and MCD spectra of MeCbl (Figure 7, bottom) also reveals that at least four bands contribute to the Abs envelope in the α/β region. However, the splitting between bands 2 and 3 ($\sim$1600 cm^{-1}) is much larger than that between bands 1 and 2 ($\sim$1080 cm^{-1}), indicating that in this case these four features cannot be members of a vibrational progression associated with a single electronic transition. The fit of the MCD spectrum in this region shows that bands 1 and 2 are oppositely signed as compared to bands 3 and 4, suggesting that these two sets of bands are members

of overlapping vibrational progressions associated with two distinct electronic transitions possessing noncollinear transition moments. This interpretation is consistent with the RR excitation profile data of MeCbl shown in Figure 6B, which also reveal the presence of two differently polarized corrin $\pi \rightarrow \pi^*$ transitions in the α/β region (vide supra).

Analysis of the D/E region of the MeCbl spectra indicates that two similarly intense transitions contribute to the Abs envelope in this region, as observed for H_2OCbl^+; however, the two transitions giving rise to the prominent CD features in the H_2OCbl^+ spectrum have no obvious counterparts in the MeCbl spectrum. The region between 26 000 and 32 000 cm^{-1} of the MeCbl Abs spectrum, corresponding to the γ region of the "typical" Cbl Abs spectrum, contains contributions from at least four similarly intense electronic transitions that have significant corrin $\pi \rightarrow \pi^*$ character, as suggested by the corresponding RR excitation profile data (Figure 6B). While each of these transitions is considerably weaker than the single intense transition dominating the γ region of "typical" Cbl Abs spectra, the integrated Abs intensity in this region is actually quite similar for H_2OCbl^+ and MeCbl.

Qualitatively, such an increase in the number of electronic transitions contributing to both the α/β and the γ regions from the "typical" to "unique" Cbl spectra suggests that the density of molecular orbitals (MOs) near the HOMO/LUMO energy gap increases upon binding of an alkyl ligand in the upper axial position of Co^{3+}Cbls. The fact that the integrated Abs intensity is roughly preserved among all Cbl species suggests that these additional donor and/or acceptor MOs available for electronic transitions are strongly mixed with corrin-based orbitals, such that the overall corrin $\pi \rightarrow \pi^*$ transition intensity is effectively distributed over a larger number of electronic transitions in alkylcobalamains.

(ii) Quantitative Band Shape Analysis for the α/β Region. A peculiar difference between the α/β regions of the "typical" and "unique" Cbl Abs spectra is that the intensity ratio of the α and β bands, assigned to the electronic origin and the first member of a vibrational progression in ν_{LA} associated with a corrin-centered $\pi \rightarrow \pi^*$ transition,[22,36] is considerably larger in the former spectrum than in the latter. This difference appears to indicate that distortions in the corresponding excited state along the ν_{LA} coordinate are substantially greater for alkylcobalamins than for other Cbl species, possibly reflecting more dramatic changes in intracorrin bonding in the former case. However, as alkylcobalamins exhibit RR spectra that reveal significant enhancement of ν_{Co-C} (e.g., see Figure 6B), their distinct Abs band shape in the α/β region might also reflect additional distortions along the Co−C coordinate. To obtain quantitative insight into the excited-state distortions associated with the corrin $\pi \rightarrow \pi^*$ transition responsible for the α/β bands in "typical" and "unique" Cbl spectra, the corresponding Abs band shapes were analyzed within the framework of time-dependent Heller theory.[82−84]

Although numerous corrin modes are observed in the RR spectra of Cbls obtained upon excitation in resonance with the α/β bands, ν_{LA} demonstrates by far the greatest enhancement in this region. Consequently, initial attempts were made to model the observed vibronic structure in the α/β region of Cbl Abs spectra including only ν_{LA}. Figure 8A shows that the α/β region of the CNCbl Abs spectrum, chosen as a representative example

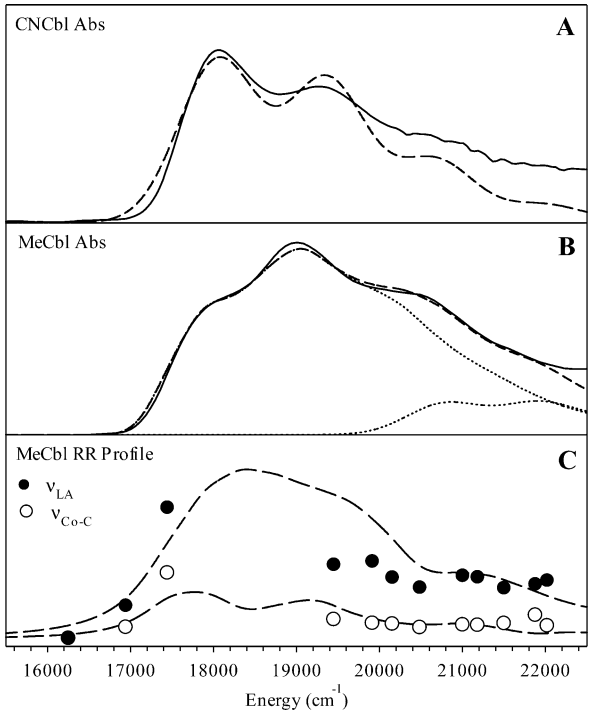

Figure 8. Time-dependent Heller theory fits (broken lines) of the experimental Abs spectra (solid lines) of CNCbl (A) and MeCbl (B) and of the RR excitation profile data (symbols) of MeCbl (C). The CNCbl Abs spectrum was modeled using a single transition, whereas the MeCbl data were modeled using two different transitions (individual bands are indicated by dotted lines). The fit parameters used for the spectral simulations can be found in Table S18.

of a "typical" Cbl Abs spectrum because of its relatively well-resolved vibrational progression in this region, is indeed reasonably well reproduced assuming excited-state distortions along this single coordinate with an excited-state frequency of 1310 cm^{-1} and $S(\nu_{LA}) = 0.82$.

Contrastingly, attempts to fit the MeCbl Abs spectrum considering a vibrational progression in ν_{LA} alone were unsuccessful, indicating that distortions along at least two coordinates must be considered. As the intensities of the other corrin-based vibrational modes relative to ν_{LA} show minor variations from species to species (Figure 5), these modes cannot be the source of the difference between the α/β regions of the "typical" and "unique" Abs spectra. Alternatively, because the 514.5-nm excited RR spectrum of MeCbl also reveals significant enhancement of ν_{Co-C} (Figure 5), we attempted to fit the α/β region of the corresponding Abs spectrum considering vibrational progressions in both ν_{LA} and ν_{Co-C} and allowing for the presence of two excited states, as required by the spectroscopic data discussed above. The relative displacements along the two coordinates were determined on the basis of the corresponding RR excitation profile data. Despite the approximate nature of this model, the agreement between experimental and simulated data is very satisfying; see Figure 8B and 8C. The fitted excited-state frequencies for ν_{LA} (1180 cm^{-1}) and ν_{Co-C} (406 cm^{-1}) are reduced by 20% relative to the ground-state frequencies, indicating that the transition corresponding to the α/β bands gives rise to considerable weakening of both corrin C=C bonds and the Co−C bond. Significantly, this analysis reveals further that the unusually large intensity of the β band relative to the α band in the "unique" Cbl Abs spectra does not necessarily reflect abnormally large excited-state distortions along ν_{LA};

rather, the corresponding Huang−Rhys parameter, $S(\nu_{LA}) = 1.05$, is only marginally larger than $S(\nu_{LA}) = 0.82$ obtained from the "typical" Abs spectrum of CNCbl (Figure 8A). Instead, in MeCbl (and presumably all other alkylcobalamins), the large relative intensity of the β band is a direct manifestation of additional distortions along the Co−C coordinate. Assuming an isolated Co−CH_3 harmonic oscillator, the fitted value of $S(\nu_{Co-C}) = 1.81$ correlates with a Co−C bond lengthening by 0.16 Å. This large increase in Co−C bond length in the excited state corresponding to the α/β bands is rather unexpected considering that these bands have traditionally been assigned to a corrin $\pi \rightarrow \pi^*$ transition. This observation lends further support to the hypothesis that the π system of the corrin macrocycle is electronically coupled to the Co−C bond, which we and others[32,87−90] formulated on the basis of RR data for MeCbl (vide supra).

3.3. Computational Data. Most computational studies of Cbls reported in the recent past were based on density functional theory (DFT) and typically relied on the success of geometry optimization to validate the methodology employed.[27,91,92] This approach has the inherent disadvantage that errors are necessarily introduced by using simplified Cbl models. Additionally, as geometry optimizations using vastly different DFT methods and basis sets typically yielded similar structures, it appears that X-ray data are inadequate for a rigorous evaluation of computations aimed at elucidation of the electronic properties of corrinoids. Instead, we have used our spectroscopic data in conjunction with the time-dependent DFT (TD-DFT) method[76−78] to evaluate calculated electronic structure descriptions of Cbl models that were based on high-resolution X-ray structural data.[54−56] This approach affords Cbl models that exactly preserve the conformation of the corrin ring imposed by outer ring substituents including the nucleotide loop and DMB, despite the fact that these substituents were not explicitly accounted for.

Evaluation Process. Initially, a series of TD-DFT calculations were performed on three distinct models of Co^{3+}Cbl species with a variety of functionals and basis sets to find the combination that yielded the best agreement between experimental and calculated Abs and CD spectra (see Experimental Section for details). The three models used differed with respect to the lower axial ligand, which was modeled as either DMB, imidazole, or amine. While in each case calculated MO descriptions using DMB or imidazole as the lower axial ligand were nearly identical and similar to those obtained for the amine model, the large size of the DMB model prevented proper treatment by the TD-DFT method, which led to poor agreement between calculated and experimental spectral data. To model key structural and electronic properties of the actual DMB ligand while reducing the number of atoms, all subsequent DFT calculations were therefore performed on Cbl models possessing an imidazole in the lower axial position.[93]

Overall, the best correspondence between calculated and experimental Abs and CD spectra of H_2OCbl^+, CNCbl, and MeCbl was achieved using the B3LYP hybrid functional[70−72] with the SV(P) split valence basis[67,73] on all atoms except cobalt for which the TZVP triple-ζ basis[66,67] was employed. While TD-DFT results obtained with the gradient-corrected PW-LDA functional[65] yielded transition energies that seemed to agree even better with experimental values, closer inspection revealed that two similarly intense transitions were predicted in the γ regions of the "typical" H_2OCbl^+ and CNCbl Abs spectra. As this prediction is inconsistent with our results from the Gaussian deconvolutions of the corresponding experimental spectra (vide supra), we present in this paper only the DFT and TD-DFT results obtained with the B3LYP hybrid functional.

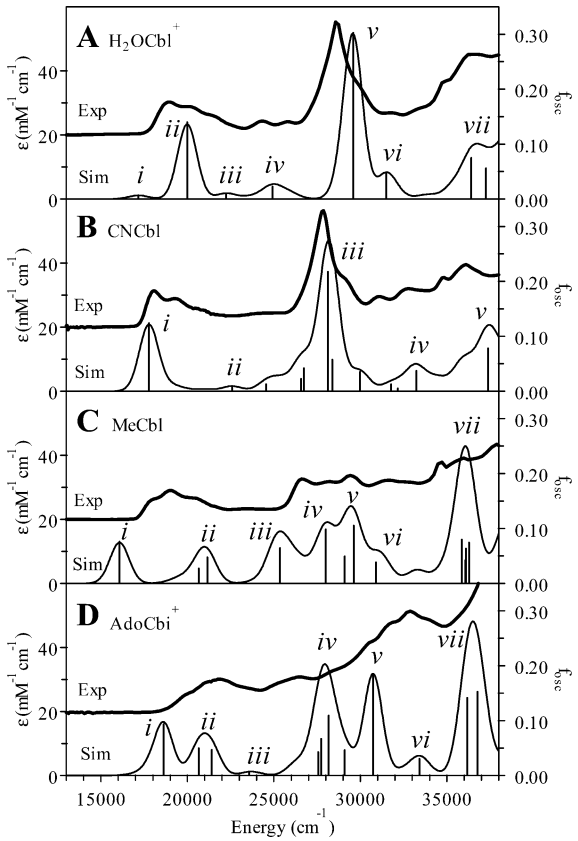

Figure 9. Experimental and TD-DFT simulated Abs spectra for H_2OCbl^+ (A), CNCbl (B), MeCbl (C), and $AdoCbi^+$ (D). The calculated spectra were uniformly red-shifted by 5500 cm^{-1} to facilitate comparison with the experimental data. The major bands in the calculated spectra are labeled *i*−*vii*, and the transitions producing the dominant contributions are indicated by solid lines (the corresponding oscillator strengths are indicated on the right-hand axis). See text and Tables 3 (H_2OCbl^+), S13 (CNCbl), 4 (MeCbl), and S17 ($AdoCbi^+$) for more details.

To facilitate comparison with our spectroscopic data, TD-DFT computed transition energies and oscillator strengths were used to simulate Abs spectra (Figure 9), assuming that each electronic transition gives rise to a Gaussian band with a full width at half maximum of $\nu_{1/2} = 1250$ cm^{-1}. In this case, the oscillator strength f and molar extinction coefficient ϵ_{max} (M^{-1} cm^{-1}) are related by $f = 4.61 \times 10^{-9}\, \epsilon_{max}\, \nu_{1/2}$.[94] All simulated spectra were then uniformly downshifted by 5500 cm^{-1} to compensate for the fact that the B3LYP TD-DFT method tends

(89) Dong, S. L.; Padmakumar, R.; Maiti, N.; Banerjee, R.; Spiro, T. G. *J. Am. Chem. Soc.* **1998**, *120*, 9947−9948.
(90) Puckett, J. M.; Mitchell, M. B.; Hirota, S.; Marzilli, L. G. *Inorg. Chem.* **1996**, *35*, 4656−4662.
(91) Jensen, M. P.; Halpern, J. *J. Am. Chem. Soc.* **1999**, *121*, 2181−2192.
(92) Jensen, M. P.; Zinkl, D. M.; Halpern, J. *Inorg. Chem.* **1999**, *38*, 2386-2393.

(93) The replacement of the DMB by an imidazole in the Cbl models requires no change in the conformation of the corrin ring, as the coordinates for all corrin atoms are taken directly from the X-ray data. As such, the frozen macrocycle maintains all steric effects imposed by outer ring substituents including the nucleotide loop and DMB, which are not explicitly included in our models.
(94) Lever, A. B. P. *Inorganic Electronic Spectroscopy*, 2nd ed.; Elsevier: Amsterdam/New York, 1984.

to overestimate transition energies.[47] With this minor adjustment, amazing agreement was achieved between calculated and experimental Abs spectra for all corrinoid species investigated (Figure 9).

H_2OCbl^+ and CNCbl. For H_2OCbl^+ and CNCbl, our TD-DFT calculations predict one intense electronic transition in the visible spectral region that is polarized along the $C^5\cdots C^{15}$ vector of the corrin ring (Figure 1) and one very intense transition in the UV that is polarized along $Co\cdots C^{10}$ vector. Thus, the calculations almost quantitatively reproduce the main characteristics of the electronic transitions responsible for the α/β bands and the γ band of "typical" Abs spectra (Figure 9A and 9B). Additional transitions of lower intensity are predicted near 25 000 cm^{-1} where the D and E bands are observed in the experimental Abs spectra (note that these features are correctly predicted to be more intense for H_2OCbl^+ than for CNCbl). Remarkably, the calculation on the H_2OCbl^+ model also successfully reproduces the weak transition that gives rise to the positive feature on the low-energy side of the α band in the experimental CD spectrum (band 1 in Figure 7, top).

MeCbl. Our TD-DFT computation on the MeCbl model (Figure 9C) suggests the presence of two intense features in the α/β region of "unique" Cbl Abs spectra, consistent with the results from the Gaussian deconvolutions of our experimental spectra (Figure 7, bottom). The lower-energy transition is predicted to be polarized along the $C^5\cdots C^{15}$ axis of the corrin macrocycle, whereas the transition moment associated with the dominant contributor to the second feature is tilted 9° away from this axis toward the $Co\cdots C^{10}$ vector. These predictions are in excellent agreement with our RR excitation profile data for MeCbl, as the intensity of ν_{SA} relative to ν_{LA} (which is a qualitative measure of $Co\cdots C^{10}$ vs $C^5\cdots C^{15}$ polarization) increases as a function of excitation energy on approaching the higher-energy feature in the α/β region (Figure 6B). Significantly, our TD-DFT calculations also successfully reproduce the dramatic changes in the γ region of the Cbl Abs spectrum upon substitution of the upper axial ligand by an alkyl group. The calculated "unique" Abs spectrum of MeCbl shows multiple bands of similar intensities in the UV region where the single intense γ band is predicted (and observed) in "typical" Cbl spectra. Several transitions with varying polarizations are contributing to these bands in the calculated MeCbl Abs spectrum, consistent with our results from the quantitative analysis of the corresponding experimental data (Figure 7, bottom).

$MeCbi^+$. Because X-ray data for cobinamides have not yet become available, key structural features of $AdoCbi^+$ were modeled as described in the Experimental Section. While our approximate $AdoCbi^+$ model actually possesses a methyl group in the upper axial position, as present in $MeCbi^+$, spectroscopic data demonstrate that a methyl group mimics the electronic properties of Ado very well: (i) Abs spectra of $AdoCbi^+$ and $MeCbi^+$ reported in the literature[88] are virtually identical, and (ii) our Abs, CD, and MCD spectra of AdoCbl and MeCbl are nearly indistinguishable (cf. Figures 3 and 4). Despite the approximations made in generating our $MeCbi^+$ model, the TD-DFT computed Abs spectrum for this species (Figure 9) agrees reasonably well with the experimental Abs spectrum of $AdoCbi^+$ (and $MeCbi^+$, see ref 88). Most importantly, our calculation correctly predicts a blue-shift by ~2500 cm^{-1} of the lowest-energy absorption feature upon substitution of the DMB (modeled by an imidazole) with H_2O in the lower axial position.

3.4. Spectral Assignments. In light of the fact that our TD-DFT computed Abs spectra for H_2OCbl^+, CNCbl, MeCbl, and $MeCbi^+$ reproduce all essential features observed in the corresponding experimental data, it is reasonable to use the DFT calculated MO descriptions as the basis for assigning key spectral features in "typical" and "unique" Abs spectra of Cbls. Figure 10 shows isosurface plots of the relevant MOs of H_2OCbl^+ (left) and MeCbl (right), which are employed here as representative examples of Cbl species displaying "typical" and "unique" Abs spectra, respectively.[95] Although the corrin macrocycle lacks any symmetry, we note from the MO plots in Figure 10 that the effective electronic symmetry is approximately C_s.[96] To infer the polarization of electronic transitions, it is therefore convenient to classify MOs according to their transformation behavior with respect to the pseudo mirror plane that is oriented perpendicular to the $C^5\cdots C^{15}$ axis and contains the $Co\cdots C^{10}$ vector (Figure 1). Transitions will be polarized roughly along the $Co\cdots C^{10}$ vector if the two MOs involved possess the same symmetry and parallel to the $C^5\cdots C^{15}$ axis otherwise.

H_2OCbl^+. While in the TD-DFT approach each electronic transition is expressed in terms of a linear combination of numerous one-electron excitations (Table 3), the transition intensity is typically governed by those donor and acceptor MOs possessing similar compositions.[97] From Figure 9A and Table 3, the transition responsible for the α/β bands in the H_2OCbl^+ Abs spectrum (band *ii*, state 3) predominantly involves one-electron excitation from the HOMO(#116) to the LUMO(#117) that are both largely localized on the corrin macrocycle (Figure 10, left). Because these two MOs possess different symmetries with respect to the pseudo mirror plane, this transition is expected to be polarized along the $C^5\cdots C^{15}$ vector. This prediction is consistent with the TD-DFT computed polarization and our spectroscopic data for H_2OCbl^+ (vide supra). Inspection of the isosurface plots reveals further that electronic excitation from the HOMO(#116) to the LUMO(#117) should strengthen some corrin C−C bonds while weakening others. This pattern agrees well with the published normal mode description for ν_{LA} (Figure 5, inset),[48] providing a rationale for the predominant enhancement of this mode in RR spectra of H_2OCbl^+ obtained for excitation in resonance with the α/β bands (Figures 5 and 6).

The dominant transition in the γ region (band υ, state 14) has large contributions from three different one-electron excitations. All three excitations are expected to be polarized roughly along the $Co\cdots C^{10}$ vector on the basis of the symmetries of the corresponding MOs (Figure 10, left), consistent with the TD-DFT computed polarization of this transition and in agreement with our spectroscopic data (vide supra). As the HOMO−1(#115) → LUMO(#117) excitation is the main contributor to a considerably weaker transition in the D/E region (see below),

(95) Isosurface plots of the relevant MOs of CNCbl and $MeCbi^+$ are presented in Figures S5 and S7, respectively.

(96) Note that the *x* and *y* axes are rotated by 45° about *z* from their usual orientations along the metal−ligand bonds. The designation of Co 3d orbitals contributing to Cbl MOs reflects this rotation.

(97) The percentages listed give the contributions of individual one-electron excitations required to model the charge distribution in the corresponding excited state. It is expected that those excitations with donor and acceptor MOs composed of similar atomic orbitals are the dominant intensity contributors to the overall transition.

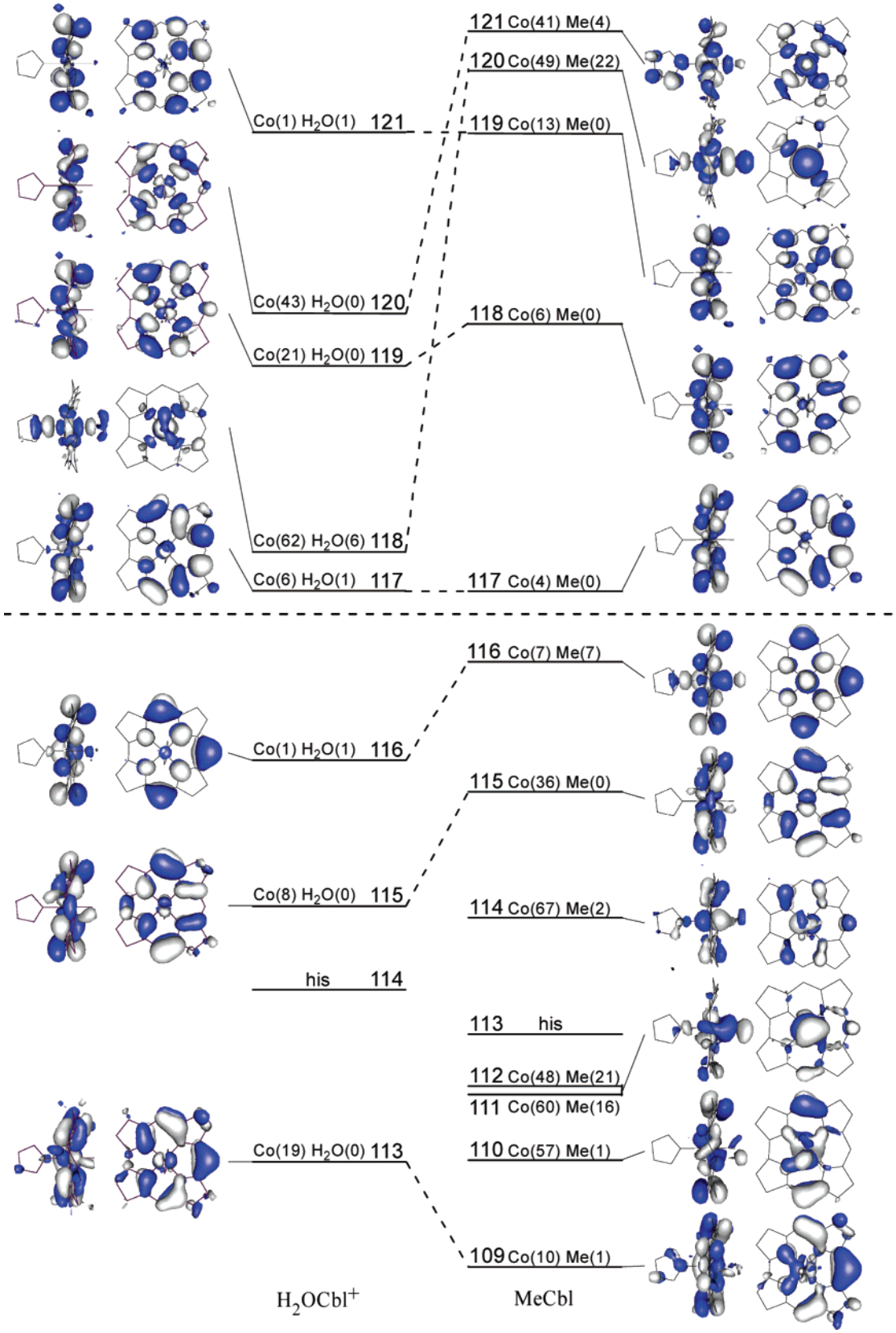

Figure 10. Isosurface plots of the relevant MOs of H_2OCbl^+ (left) and MeCbl (right). MOs are arranged according to their calculated energies with the doubly occupied orbitals shown below the horizontal dashed line (note that the HOMO/LUMO gap is not drawn to scale). The percent contributions from the Co 3d orbitals and the 2s and 2p orbitals of the coordinating atom from the upper axial ligand to each MO are given in parentheses.

the high intensity of the γ band must originate from the one-electron excitations from the HOMO(#116) to the nearly degenerate set of corrin π^*/Co $3d_{xy}$-based MOs (#119 and #120). Note that this transition primarily corresponds to a corrin $\pi \rightarrow \pi^*$ excitation with negligible corrin $\pi \rightarrow$ Co $3d_{xy}$ charge-transfer character, as revealed by the TD-DFT calculated eigenvector

Table 3. TD-DFT Calculated Energies (in cm^{-1}), Percent Contributions from Dominant One-Electron Excitations, and Oscillator Strengths for the Major Electronic Transitions of H_2OCbl^+ (Band Designations Relate to Figure 9A)

band	state	E (cm^{-1})	f	transition	%	donor MO	acceptor MO	notes[a]
i	3	17 175	0.0068	116 → 118	86	cor-π (HOMO)	Co $3d_{z^2}$	LMCT
ii	4	19 985	0.1398	116 → 117	83	cor-π (HOMO)	cor-π* (LUMO)	LA
iii	5	22 230	0.0105	111 → 120	17	cor-π	Co $3d_{xy}$	CT
				116 → 120	16	cor-π (HOMO)	Co $3d_{xy}$ }	SA[b]
				116 → 119	12	cor-π (HOMO)	Co $3d_{xy}$ }	
iv	8	24 925	0.0227	115 → 117	48	cor-π	cor-π* (LUMO)	SA
				116 → 120	26	cor-π (HOMO)	Co $3d_{xy}$	LMCT
v	14	29 575	0.3026	116 → 119	26	cor-π (HOMO)	Co $3d_{xy}$ }	SA[b]
				116 → 120	23	cor-π (HOMO)	Co $3d_{xy}$ }	
				115 → 117	18	cor-π	cor-π* (LUMO)	SA
vi	16	31 505	0.0463	116 → 121	35	cor-π (HOMO)	cor-π*	LA
				113 → 117	20	cor-π	cor-π* (LUMO)	LA
				115 → 119	18	cor-π	Co $3d_{xy}$ }	LA[b]
				115 → 120	14	cor-π	Co $3d_{xy}$ }	
vii	24	36 410	0.0745	109 → 118	26	Co 3d/cor-π	Co $3d_{z^2}$	d → d
				112 → 118	11	his-π/cor-π	Co $3d_{z^2}$	CT
	26	37 260	0.0559	112 → 117	15	his-π/cor-π	cor-π* (LUMO)	CT
				109 → 117	14	Co 3d/cor-π	cor-π* (LUMO)	CT
				116 → 121	11	cor-π (HOMO)	cor-π*	SA

[a] Information concerning the type and/or polarization (short-axis (SA) or long-axis (LA) polarized) of the corresponding one-electron excitation. [b] Transitions evenly comprised of two excitations each originating from the same donor MO and terminating in MO#119 and MO#120, respectively, have little charge-transfer character.[98]

of the corresponding excited state (i.e., the contributions from the HOMO(#116) → MO#119 and MO#120 one-electron excitations to this eigenvector are oppositely signed, which effectively cancels out the corrin $\pi \rightarrow$ Co $3d_{xy}$ charge-transfer contributions to the excited state).[98]

Our TD-DFT calculation for H_2OCbl^+ also provides insight into the origin of more subtle features in the experimental Abs and CD spectra. The most intense transition in the D/E region is predicted to possess significant contributions from two distinct one-electron excitations (band *iv*, state 8); however, inspection of the MO plots (Figure 10, left) suggests that the corrin-centered HOMO−1(#115) → LUMO(#117) excitation polarized along the Co···C[10] vector produces the dominant contribution to the Abs intensity in this region. The computational data suggest further that the weak positive feature observed on the low-energy side of the α band in the experimental CD spectrum (band 1 in Figure 7, top) arises from a transition that mainly involves HOMO(#116) → LUMO+1(#118) excitation and thus formally corresponds to a corrin $\pi \rightarrow$ Co $3d_{z^2}$ charge-transfer (CT) transition (band *i*, state 1). Because this transition involves donor and acceptor MOs of vastly different compositions (Figure 10, left), it carries very low electric dipole intensity and is therefore difficult to discern in the experimental Abs spectrum. However, the involvement of the Co $3d_{z^2}$-based MO presumably induces considerable magnetic dipole character into this transition, thus allowing for its observation in the experimental CD spectrum.

CNCbl. Our TD-DFT results for CNCbl are very similar to those obtained for H_2OCbl^+ (Figure S5 and Table S13), as expected on the basis of the high similarity of the corresponding experimental and calculated Abs spectra (Figure 9). The transition responsible for the α/β bands in the CNCbl Abs spectrum also primarily involves HOMO → LUMO excitation and is essentially localized on the corrin macrocycle. Likewise, the dominant transition in the γ region again originates from the HOMO and terminates in a corrin-based π* MO that is in nature similar to the corrin π* orbital contributing to MOs #119 and #120 of H_2OCbl^+. The fact that the transitions responsible for the α/β bands and the γ band downshift by similar amounts from H_2OCbl^+ to CNCbl is due to the greater σ-donor strength of cyanide as compared to that of H_2O. In CNCbl, the HOMO has a significantly greater contribution (1.5% vs 0.2% in H_2OCbl^+) from the formally unoccupied Co $3d_{z^2}$ orbital, which induces a strong σ-antibonding interaction between Co and the lower axial base. This additional antibonding interaction raises the energy of the HOMO, thus uniformly shifting electronic transitions originating from this orbital to lower energy. However, the greater σ-donor strength of cyanide as compared to H_2O most dramatically destabilizes the $3d_{z^2}$-based MO. Consequently, the transition from the HOMO to the Co $3d_{z^2}$-based MO, which is responsible for the low-energy feature in the H_2OCbl^+ CD spectrum (band 1 in Figure 7, top), is calculated to shift by ∼7400 cm^{-1} to higher energy in the CNCbl spectra where it is predicted to occur in the D/E region.

MeCbl. Figure 10 (right) shows the relevant portion of the calculated MO diagram for MeCbl. Comparison with the MO diagram for H_2OCbl^+ (Figure 10, left) reveals an almost one-to-one correspondence between the corrin-based MOs with respect to relative energies and compositions. However, the H_2OCbl^+ and MeCbl MO diagrams exhibit some key differences that provide insight into the factors that distinguish Cbl species exhibiting "typical" Abs spectra from those displaying "unique" spectra. Most importantly, from H_2OCbl^+ to MeCbl the number of occupied MOs near the HOMO increases considerably, as anticipated on the basis of our spectral analysis (section 3.2). All of these additional MOs (#110−112 and #114) possess primarily Co 3d character, and two of them (#111 and #112) also have large contributions from the methyl C $2p_z$ orbital. This

(98) In CNCbl, the corrin π* and Co 3d orbitals that produce the dominant contributions to MOs #119 and #120 of H_2OCbl^+ are considerably separated in energy, which greatly reduces the extent of mixing between the two. As a result, the intensity of the γ transition for CNCbl is predicted to be governed by a single one-electron excitation, from the HOMO to a corrin π*-based MO that largely resembles the corrin π* orbital contributing to MOs #119 and #120 of H_2OCbl^+ (see Figure S5 and Table S13).

Table 4. TD-DFT Calculated Energies (in cm^{-1}), Percent Contributions from Dominant One-Electron Excitations, and Oscillator Strengths for the Major Electronic Transitions of MeCbl (Band Designations Relate to Figure 9C)

band	state	E (cm^{-1})	f	transition	%	donor MO	acceptor MO	notes[a]
i	1	16 075	0.0760	116 → 117	89	cor-π (HOMO)	cor-π* (LUMO)	LA
ii	5	20 660	0.0273	115 → 117	51	Co $3d_{yz}$/cor-π	cor-π* (LUMO)	SA
				116 → 118	18	cor-π (HOMO)	cor-π*	SA
	6	21 165	0.0472	114 → 117	78	Co $3d_{xz}$	cor-π* (LUMO)	MLCT/LA
iii	9	25 355	0.0643	116 → 118	30	cor-π (HOMO)	cor-π*	SA
				115 → 118	15	Co $3d_{yz}$/cor-π	cor-π*	LA
				110 → 117	11	Co 3d	cor-π* (LUMO)	MLCT/SA
iv	14	28 005	0.0983	115 → 118	26	Co $3d_{yz}$/cor-π	cor-π*	LA
				116 → 121	16	cor-π (HOMO)	Co $3d_{xy}$	LMCT
				112 → 117	14	Co 3d/C_{met} $2p_z$	cor-π* (LUMO)	MLCT
				111 → 117	12	Co 3d/C_{met} $2p_z$	cor-π* (LUMO)	MLCT
v	15	29 090	0.0490	114 → 118	40	Co $3d_{xz}$	cor-π*	MLCT
				110 → 117	14	Co 3d	cor-π* (LUMO)	MLCT/SA
	16	29 620	0.1052	116 → 120	36	cor-π (HOMO)	Co $3d_{z^2}$/C_{met} $2p_z$	LMCT
				110 → 117	19	Co 3d	cor-π* (LUMO)	MLCT/SA
vi	17	30 890	0.0385	116 → 119	44	cor-π (HOMO)	cor-π*	LA
				116 → 121	14	cor-π (HOMO)	Co $3d_{xy}$	LMCT
				109 → 117	10	cor-π	cor-π* (LUMO)	LA
vii	25	35 855	0.0799	108 → 117	26	his-π/cor-π	cor-π* (LUMO)	CT
				112 → 118	22	Co 3d/C_{met} $2p_z$	cor-π*	MLCT
				111 → 118	17	Co 3d/C_{met} $2p_z$	cor-π*	MLCT
	26	36 075	0.0427	114 → 119	46	Co $3d_{xz}$	cor-π*	MLCT
				108 → 117	18	his-π/cor-π	cor-π* (LUMO)	CT
				114 → 121	14	Co $3d_{xz}$	Co $3d_{xy}$	d → d
	27	36 110	0.0631	108 → 117	23	his-π/cor-π	cor-π* (LUMO)	CT
				115 → 122	22	Co $3d_{yz}$/cor-π	his-π*	CT
				114 → 119	12	Co $3d_{xz}$	cor-π*	MLCT/LA
				115 → 121	10	Co $3d_{yz}$/cor-π	Co $3d_{xy}$	d → d
	28	36 295	0.0744	115 → 122	46	Co $3d_{yz}$/cor-π	his-π*	CT
				108 → 117	14	his-π/cor-π	cor-π* (LUMO)	CT
				111 → 118	12	Co 3d/C_{met} $2p_z$	cor-π*	MLCT

[a] Information concerning the type and/or polarization (short-axis (SA) or long-axis (LA) polarized) of the corresponding one-electron excitation.

result indicates that in MeCbl and, by analogy, alkylcobalamins in general, transfer of electron density from the strongly σ-donating alkyl ligand to the Co center greatly lowers the effective nuclear charge of the metal ion, thereby raising the energies of all Co 3d orbitals. With this important difference in electronic properties of the upper axial ligands in H_2OCbl^+ and MeCbl in mind, interpretation of the "unique" Cbl Abs spectrum becomes relatively straightforward.

From Figure 9C and Table 4, the transition associated with the α/β bands in the MeCbl Abs spectrum again predominantly involves one-electron excitation from the HOMO(#116) to the LUMO(#117); however, the HOMO of MeCbl differs from that of H_2OCbl^+ (Figure 10) by having significant contributions from the formally unoccupied Co $3d_{z^2}$ orbital (6.7%) and the methyl C $2p_z$ orbital (6.1%). While the Co $3d_{z^2}$ orbital is strongly σ-antibonding to the N $2p_z$ orbital of the axial base, which leads to a considerable destabilization of the HOMO of MeCbl relative to H_2OCbl^+ (hence the lower energy of the α/β bands), it is σ-bonding with respect to the Co−CH_3 bond. Because the LUMO has no contributions from the methyl group, the HOMO(#116) → LUMO(#117) transition, formally corresponding to a corrin $\pi \rightarrow \pi^*$ excitation, would be expected to significantly weaken the Co−CH_3 bond. This prediction is in excellent agreement with the strong enhancements of both ν_{LA} and ν_{Co-C} in RR spectra of MeCbl (as opposed to the almost exclusive enhancement of ν_{LA} in RR spectra of H_2OCbl^+) obtained for excitation in resonance with the α/β bands; see Figures 5 and 6.

Our computational data for MeCbl suggest further that the second intense feature observed in the α/β region of the experimental Abs spectrum (modeled by bands 3 and 4 in Figure 7, bottom) has substantial contributions from two distinct electronic transitions (band *ii*, states 5 and 6). The lower-energy transition primarily involves excitation of an electron from the HOMO−1(#115) to the LUMO(#117), analogous to the most intense transition calculated in the D/E region of the H_2OCbl^+ Abs spectrum. The downshift of this transition in the MeCbl spectrum is due to a substantial increase in Co 3d-orbital character in the corrin-based donor MO and the consequent increase in Co−N(corrin) π-antibonding interactions that raise this MO in energy. The higher-energy transition contributing to band *ii* in the calculated MeCbl Abs spectrum (Figure 9C) involves almost pure HOMO−2(#114) → LUMO(#117) electronic excitation, formally corresponding to a Co $3d_{xz} \rightarrow$ corrin π^* CT transition.[99] The one-electron excitation producing the dominant contribution to the γ region of the "typical" Abs spectra of H_2OCbl^+ and CNCbl corresponds to the HOMO(#116) → LUMO+1(#118) transition of MeCbl. Table 4 reveals that this one-electron excitation is the principal contributor to the transition responsible for band *iii* in the calculated MeCbl Abs spectrum (state 9). However, as the corresponding transition also has significant Co 3d → corrin π^* CT character, the actual contribution from the HOMO(#116) → LUMO+1(#118) excita-

(99) The relatively high intensity of this transition derives from the fact that the corrin C and N 2p orbitals contributing to the donor MO (#114) are also the main contributors to the acceptor MO (#117).

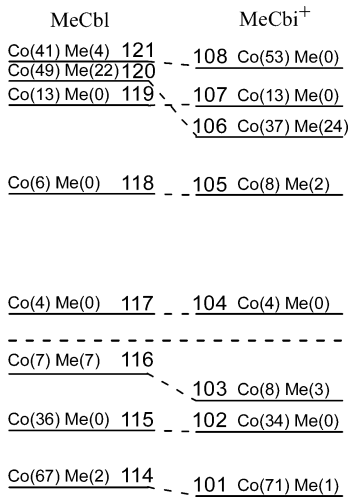

Figure 11. Relevant portions of the calculated MO diagrams for MeCbl and $MeCbi^+$, vertically shifted to match the LUMO energies (note that the HOMO/LUMO gap is not drawn to scale). Doubly occupied MOs are shown below the horizontal dashed line. The percent contributions from the Co 3d and methyl 2p orbitals to each MO are given in parentheses.

tion is reduced, leading to the lower intensity of this transition in the "unique" than in "typical" Cbl Abs spectra. It is interesting to note that on the basis of these spectral assignments, the trend that the α and γ bands tend to shift uniformly in "typical" Cbl Abs spectra as a function of the σ-donor strength of the upper axial ligand also extends to "unique" spectra where the "γ band" now corresponds to the lowest-energy, relatively prominent Abs feature in the perturbed γ region (band 7, Figure 7, bottom). The presence of additional intense features in the γ region of the calculated MeCbl Abs spectrum is another manifestation of the close energetic proximity of the occupied Co 3d and corrin π orbitals that are therefore strongly mixed. As a result of this extensive mixing, all occupied MOs of MeCbl directly beneath the HOMO have considerable corrin π orbital character (Figure 10, right) and are thus available for relatively intense electronic transitions involving unoccupied corrin π*-based acceptor MOs.

$MeCbi^+$. Many of the features discussed for the MeCbl Abs spectrum are preserved upon substitution of the lower axial base by a water molecule, as present in $MeCbi^+$. As anticipated on the basis of the weaker σ-donor strength of a water molecule as compared to imidazole (or DMB), the most dramatic change in the calculated electronic structure between MeCbl and $MeCbi^+$ involves a large stabilization by ~0.5 eV of the unoccupied Co $3d_{z^2}$-based MO (Figure 11). The relative energies of the HOMOs for MeCbl and $MeCbi^+$ are also affected by the σ-antibonding strength of the lower axial ligand, as for both systems the HOMO contains significant Co $3d_{z^2}$ character. Specifically, the HOMO undergoes a large stabilization (~0.2 eV) upon substitution of the axial base with a water molecule. Consequently, all electronic transitions originating from the HOMO occur at considerably higher energy in $MeCbi^+$ than in MeCbl, whereas those terminating in the Co $3d_{z^2}$-based MO shift to lower energy.

On the basis of this qualitative bonding analysis, key spectral differences between MeCbl and $MeCbi^+$ are readily understood. The HOMO → LUMO transition, responsible for the α/β bands in the MeCbl Abs spectrum, is predicted to shift 2550 cm^{-1} to higher energy in the $MeCbi^+$ spectrum (band *i* in Figure 9D). As the two transitions responsible for the higher-energy feature in the α/β region of the calculated MeCbl Abs spectrum do not involve the HOMO, their energies and intensities remain similar in the computed $MeCbi^+$ Abs spectrum (cf. band *ii* in Figure 9C and 9D). Thus, the weakly structured lowest-energy Abs feature observed for $MeCbi^+$ presumably has contributions from several electronic transitions, including those responsible for the α/β bands and the dominant feature in the D/E region of "typical" Cbl Abs spectra. Support for this proposal is provided by our experimental CD and MCD data of $AdoCbi^+$ (Figure 4), which show the presence of numerous features in this region that are associated with at least four different electronic transitions based on their respective signs in the two spectra (Figure S3).

The higher-energy region of the computed $MeCbi^+$ Abs spectrum (bands *iv*−*vi*, Figure 9D) involves one-electron excitations similar to those contributing to bands *iii*−*vi* in the calculated MeCbl Abs spectrum. However, in going from MeCbl to $MeCbi^+$, the Co $3d_{z^2}$ orbital drops in energy and thus interacts more strongly with the unoccupied corrin π*-based MOs near the LUMO; therefore, no simple correlation exists between electronic transitions responsible for the dominant features of the MeCbl and $MeCbi^+$ Abs spectra in this region.

4. Discussion

Spectroscopic data of corrinoids reported in the literature are abundant. However, despite numerous decades of intensive investigations of the B_{12} cofactors MeCbl and AdoCbl, their "unique" Abs spectra remained largely unassigned.[22] Likewise, geometric and electronic factors distinguishing Cbl species exhibiting "typical" Abs spectra, such as H_2OCbl^+ and CNCbl (vitamin B_{12}), from those displaying "unique" Abs spectra, which includes all alkylcobalamins, had yet to be explored. In this study, we have used a combination of complementary spectroscopic tools to probe the excited electronic states of representative Cbl species exhibiting "typical" and "unique" Abs spectra. Our combined analysis of Abs, CD, and MCD spectra as well as RR excitation profile data has afforded a suitable basis for a rigorous evaluation of DFT electronic structure calculations on approximate Cbl models that possess the actual corrin ring. Using the B3LYP hybrid functional, we achieved almost quantitative agreement between experimental and TD-DFT calculated Abs spectra for all species included in this study (Figure 9). Together, our spectroscopic/computational studies provide significant new insight into the spectral and electronic properties of the B_{12} cofactors and some of their naturally occurring precursors. Below, key findings from these studies are briefly discussed, and their implications for biological Co−C bond activation are explored.

Cbl Species Exhibiting "Typical" Abs Spectra. Consistent with previous assignments,[22,47] our TD-DFT-assisted analysis of the "typical" H_2OCbl^+ and CNCbl Abs spectra (Figure 3) reveals that the α and β bands correspond to the electronic origin and the first member of a progression in ν_{LA} (depicted in the inset of Figure 5) associated with the corrin-based HOMO → LUMO transition that is polarized along the $C^5\cdots C^{15}$ vector (Figure 1). The isosurface plots in Figure 10 suggest that electronic excitation from the HOMO to the LUMO modulates the strengths of corrin C−C bonds such as to induce distortions of the macrocycle that agree well with the published normal mode description for ν_{LA}.[48] The single intense transition responsible for the prominent γ band in the H_2OCbl^+ and CNCbl

Abs spectra is also attributed to a corrin-based $\pi \rightarrow \pi^*$ transition originating from the HOMO. The primary acceptor orbital in this transition is a corrin π^* orbital (the major contributor to MOs #119 and #120 of H_2OCbl^+; see Figure 10, left) that has the same symmetry as the HOMO with respect to the pseudo C_s mirror plane of the corrin macrocycle. This results in a transition moment that is oriented roughly along the Co···C^{10} vector and thus in predominant RR enhancement of ν_{SA} for excitation in resonance with the γ band (Figures 5 and 6). Last, the most intense transition in the D/E region is assigned to a corrin-based $\pi \rightarrow \pi^*$ transition from the HOMO−1 to the LUMO (corresponding to MOs #115 and #117 of H_2OCbl^+, Figure 10, left) that is polarized along the Co···C^{10} vector.

As cyanide is a much stronger σ-donor than a water molecule, our DFT calculations predict that the Co $3d_{z^2}$-based MO is considerably raised in energy in CNCbl relative to H_2OCbl^+, consistent with the ∼1.42 V lower reduction midpoint potential of the former.[100,101] Additionally, the contribution from the formally unoccupied Co $3d_{z^2}$ orbital to the corrin-based HOMO increases from 0.2% in H_2OCbl^+ to 1.5% in CNCbl. This partial population of the Co $3d_{z^2}$ orbital induces a strong σ-antibonding interaction between the cobalt and the coordinated nitrogen of the lower axial base (N_{ax}), thereby raising the energy of the HOMO and lowering the energies of electronic transitions originating from this orbital. Thus, our DFT calculations afford an intuitively appealing model which explains the long-established trend that the α/β and γ bands in "typical" Cbl Abs spectra uniformly shift to lower energy with increasing σ-donor strength of the upper axial ligand.[22]

Cbl Species Exhibiting "Unique" Abs Spectra. Binding of an alkyl ligand in the upper axial position of Cbls, as in MeCbl or AdoCbl, results in the appearance of a significantly perturbed, "unique" Cbl Abs spectrum (Figures 3 and 4). Our DFT computations on MeCbl indicate that these spectral changes reflect the increased σ-donor strength of the alkyl ligand and the consequent destabilization of all Co 3d orbitals. As a result, the occupied Co 3d orbitals of MeCbl and, presumably, alkylcobalamins in general, shift close in energy to the HOMO (Figure 10, right), which gives rise to (i) a net increase in the number of donor MOs available for electronic transitions and (ii) extensive mixing between Co 3d and corrin π orbitals (note that while cyanide is also a relatively strong σ-donor, the occupied Co 3d orbitals of CNCbl are considerably stabilized in energy due to Co 3d → CN π^* back-bonding). It is the combination of these two effects that is responsible for the "unique" Abs spectra of alkylcobalamins.

In accordance with Cbls exhibiting a "typical" Abs spectrum, the α/β bands in the spectra of MeCbl and AdoCbl (Figures 3 and 4) are also assigned to the HOMO → LUMO transition polarized along the C^5···C^{15} vector; the additional small red-shift from CNCbl to MeCbl again correlates well with a further decrease in reduction midpoint potential by 0.07 V[101] due to the increased σ-donor strength of the methyl group. However, in this case, the corrin-based HOMO (#116, Figure 10, right) also has significant Co−C σ-bonding character. As this bonding character is lost upon HOMO → LUMO excitation, simultaneous distortions along both the ν_{LA} and the ν_{Co-C} coordinates occur in the corresponding excited state, as verified experimentally by our RR data (Figures 5B and 6B). Notably, the increase in intensity of the β band relative to the α band from "typical" to "unique" Cbl Abs spectra is a direct manifestation of this additional excited-state distortion, which lengthens the Co−C bond by ∼0.16 Å. The second intense feature in the α/β region of the MeCbl Abs spectrum (modeled by bands 3 and 4 in Figure 7) is predicted to have substantial contributions from two distinct electronic transitions: one in nature similar to the dominant transition in the D/E region of the H_2OCbl^+ Abs spectrum (involving MOs #115 and #117 of MeCbl, Figure 10, right), and one formally corresponding to a Co $3d_{xz} \rightarrow$ corrin π^* CT transition (MOs #114 and #117). The presence of numerous intense features in the γ region of "unique" Cbl Abs spectra is another consequence of the extensive mixing between occupied Co 3d and corrin π orbitals in alkylcobalamins. This mixing leads to an increase in the number of relatively intense electronic transitions in the UV region and results in a distribution of the Abs intensity contained in the γ band of "typical" Abs spectra over several different features in the "unique" spectra (Figure 9).

The greater σ-donor strength of the upper axial ligand in MeCbl as compared to CNCbl and H_2OCbl^+ leads to a further increase in Co $3d_{z^2}$ orbital character in the corrin-based HOMO to 6.7% (Figure 10, right), thereby inducing an even stronger Co−N_{ax} σ-antibonding interaction. As a result, the DFT calculated Co−N_{ax} bond order obtained from a Mayer population analysis decreases from 0.65 in H_2OCbl^+ to 0.42 in CNCbl and 0.35 in MeCbl. These values correlate nicely with the experimental Co−N_{ax} bond lengths that increase from 1.925 Å in H_2OCbl^+ [56] to 2.041 Å in CNCbl[54] and 2.162 Å in MeCbl.[54] Consequently, the same model used to explain shifts in the α band position can be invoked to rationalize the observed lengthening of the Co−N_{ax} bond with increasingly stronger σ-donors in the upper axial position, referred to as the "inverse trans effect".[29]

Effects of Axial Base on Cbl Spectral and Electronic Properties. Removal of the DMB base from MeCbl or AdoCbl to generate the corresponding Cbi that instead binds a water molecule in the lower axial position causes a blue-shift of the lowest-energy Abs feature by ∼2000 cm^{-1}. Our computations on $MeCbi^+$ indicate that this shift is due to the lower donor strength of the water ligand as compared to that of DMB, which eliminates the σ-antibonding interaction that exists between the Co $3d_{z^2}$ orbital and the lower axial ligand in the HOMO of MeCbl (Figure 10, right). Consequently, from MeCbl to $MeCbi^+$ the HOMO drops in energy by ∼0.2 eV, and electronic transitions originating from this MO shift by ∼2000 cm^{-1} to higher energy. Additionally, the "redox-active" Co $3d_{z^2}$-based MO is calculated to decrease in energy by ∼0.5 eV, which correlates well with the observed increase in reduction midpoint potential of 0.2−0.6 V upon substitution of DMB by a water molecule.[33,102]

Most importantly, however, is that despite these spectral and electronic differences between MeCbl and $MeCbi^+$, the nature of the Co−C bond is largely unperturbed. According to a Mayer population analysis,[103−105] the calculated Co−C bond order

(100) Jaselskis, B.; Diehl, H. *J. Am. Chem. Soc.* **1954**, *76*, 4345−4348.
(101) Muller, O.; Muller, G. *Biochem. Z.* **1962**, *336*, 299.
(102) Tackett, S. L.; Collat, J. W.; Abbott, J. C. *Biochemistry* **1963**, *2*, 919−923.
(103) Mayer, I. *Chem. Phys. Lett.* **1983**, *97*, 270−274.
(104) Mayer, I. *Int. J. Quantum Chem.* **1984**, *26*, 151.
(105) Mayer, I. *Theor. Chim. Acta* **1985**, *67*, 315−322.

merely decreases by ~1%. This result is consistent with published RR and IR vibrational data for alkylcobalamins that also reveal negligible changes in the Co−C bond strength upon substitution of the lower axial base by a water molecule.[90] Thus, while the strength of the $Co-N_{ax}$ bond is significantly modulated by the upper axial ligand, the nature of the Co−C bond changes little as a function of the lower axial ligand.[106] The electronic origin of this puzzling finding and possible implications for the mechanism of B_{12}-dependent enzymes will be explored in the last section.

Nature's Choice of Co/Corrin over Fe/Porphyrin. The presence of both the cobalt and the corrin macrocycle in the B_{12} cofactors is unique in biology and represents a fascinating contrast to the ubiquitous heme cofactors that contain an iron ligated by a porphyrin ligand. It has been proposed that the increased flexibility of the corrin ring may allow B_{12}-dependent enzymes to activate the Co−C bond by modulating the conformation of this macrocycle in such a way as to induce steric interactions with the upper axial ligand.[2,19] However, such a mechanism is not selective for heterolysis versus homolysis of the organometallic bond, nor does it apply to MeCbl because the methyl group is too small for a direct interaction with the corrin ring. While ongoing computational investigations in our lab do indicate that changing the planarity of the corrin macrocycle is indeed energetically feasible, this structural perturbation has remarkably little effect on the electronic properties of alkylcobalamins as a whole and the Co−C bond in particular. This result is consistent with X-ray data of CNCbl,[54] which have shown that the corrin ring can adopt an array of markedly different conformations without perturbing the length of either axial ligand.

As the conformational flexibility of the corrin ring alone does not appear to be the main reason for nature to equip the B_{12} cofactors with this exquisite ligand, electronic factors are also expected to play an important role in making this choice. While studies on B_{12}-dependent enzymes are in progress to address this issue, it is interesting to note that on the basis of our DFT computations, the frontier MOs of MeCbl possess significant Co 3d orbital character due to extensive σ-donation of electron density from the alkyl ligand (Figure 10, right), where the large contributions of the Co $3d_{z^2}$ and methyl C $2p_z$ orbitals to the corrin-based HOMO(#116) are particularly intriguing. It is tempting to speculate that the specific combination of the Co ion and the monoanionic corrin macrocycle in MeCbl and AdoCbl allow for the formation of a delicately tuned source of a methyl cation and an Ado• radical, respectively, that can be activated through substrate binding to B_{12}-dependent enzymes. Other metals would likely possess d orbitals that are too high or low in energy with respect to the "lone-pair" of electrons on the alkyl group, thus forming too weak or too strong of an organometallic bond. Alternatively, as the porphyrin ligand is a dianion, its highest-energy occupied MOs are considerably raised in energy relative to those of the corrin macrocycle. Consequently, in porphyrin analogues of the B_{12} cofactors, we would expect (i) contributions from the Co $3d_{z^2}$ and methyl C $2p_z$ orbitals to the HOMO to be greatly reduced or completely absent, and (ii) the Co^{2+}/Co^{1+} redox couple to drop below the physiologically relevant range, thus preventing methyl-transfer reactions and adenosylation (a key step in AdoCbl biosynthesis that involves transient formation of a Co^{1+}Cbl nucleophile[51,52]) from occurring.

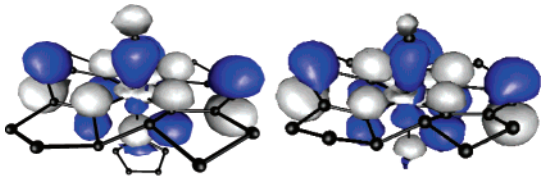

Figure 12. Comparison of isosurface MO plots for the HOMOs of MeCbl (left) and $MeCbi^+$ (right), corresponding to MOs #116 and #103, respectively (see Figure 11). Note that the large orbital contributions from the cobalt and the axial ligands reflect the strong mixing between the methyl C $2p_z$-based MO and the HOMO of the corrin macrocycle in these species.

Nature of the Co−C Bond and Implications for Co−C Bond Activation. The mechanism by which MeCbl- and AdoCbl-dependent enzymes activate the Co−C bond of the bound cofactor to produce a methyl cation and an Ado• radical, respectively, is an enduring subject of intense research.[2,8,19,32,107−109] In deciphering possible pathways for Co−C bond activation, understanding the nature of this unique bioorganometallic bond is integral. Our DFT-generated electronic-structure description for MeCbl indicates that the $Co-CH_3$ bond is very covalent in nature, as revealed by the large methyl C $2p_z$ orbital character of 22% in the unoccupied Co $3d_{z^2}$-based MO (#120 in Figure 10, right). Because the methyl C $2p_z$-derived occupied counterpart (i.e., the Co−C σ-bonding MO) is in close energetic proximity to the corrin-based HOMO, these two MOs are strongly mixed. Consequently, the HOMO of MeCbl exhibits substantial Co−C σ-bonding character (Figure 12, left), thus potentially offering one the opportunity to modulate the properties of the organometallic bond through corrin ring deformations. However, because this electronic coupling only involves weak π-interactions, conformational changes of the corrin macrocycle are not expected to perturb the $Co-CH_3$ bond to any significant degree (see also our discussion in the previous section).

A puzzling and hitherto poorly understood result from previous studies of corrinoids is that while the identity of the upper axial ligand has a great effect on the $Co-N_{ax}$ bond strength, the lower axial ligand does not appreciably modulate the Co−C bond strength. Significantly, our DFT computations also provide a simple explanation for this phenomenon. The isosurface plots in Figure 12 reveal that the contributions from the formally unoccupied Co $3d_{z^2}$ orbital and the methyl C $2p_z$ orbital (the "lone-pair" of electrons) to the HOMOs of MeCbl and MeCbi are nearly identical, which is expected on the basis of the fact that this interaction involves two orbitals of relatively similar energies that are destabilized considerably relative to the N $2p_z$ orbital of the axial base. Alternatively, the degree of $Co-N_{ax}$ σ-antibonding character is directly determined by the extent of σ-donation of electron density from the upper axial

(106) Co−C bond strength is governed by the curvature of the Co−C potential energy surface at its minimum. The Co−C bond dissociation energy (BDE) corresponds to the energy difference between the final (Co^{2+}Cbl/Co^{2+}Cbi) and initial (AdoCbl/$AdoCbi^+$) states. Thus, reports of an increased Co−C BDE for $AdoCbi^+$ as compared to that for AdoCbl are not inconsistent with our computations that suggest a similar Co−C bond strength in the two species, in nice agreement with published RR and IR data.

(107) Chowdhury, S.; Banerjee, R. *J. Am. Chem. Soc.* **2000**, *122*, 5417−5418.
(108) Brown, K. L.; Zou, J. *J. Am. Chem. Soc.* **1998**, *120*, 9466−9474.
(109) Kräutler, B.; Keller, W.; Kratky, C. *J. Am. Chem. Soc.* **1989**, *111*, 8936−8938.

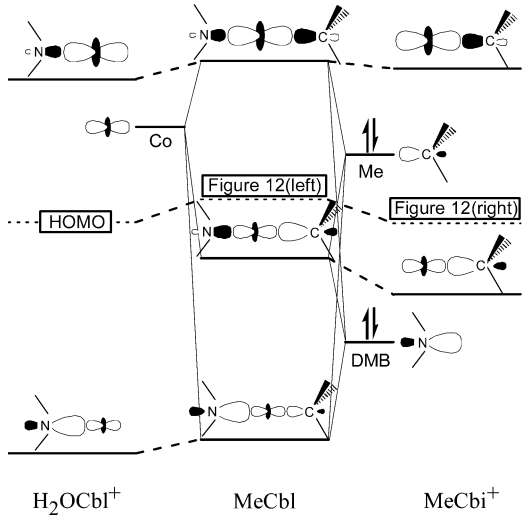

Figure 13. Qualitative correlation diagram describing the bonding interactions between the cobalt center and the axial ligands for H_2OCbl^+ (left), MeCbl (center), and $MeCbi^+$ (right). Also included are the approximate positions of the corresponding HOMOs (dotted lines). Isosurface plots of the HOMOs of MeCbl and $MeCbi^+$ are shown in Figure 12 and of H_2OCbl^+ in Figure 10, left.

ligand into the Co $3d_{z^2}$ orbital. Figure 13 shows a qualitative MO diagram that summarizes these axial bonding interactions for H_2OCbl^+, MeCbl, and $MeCbi^+$. While substitution of the upper axial ligand from H_2OCbl^+ to MeCbl induces a substantial $Co-N_{ax}$ σ-antibonding interaction, replacement of the lower axial ligand from MeCbl to MeCbi has virtually no effect on the Co−C bond (i.e., the bond order does not change, as both occupied MOs are σ-bonding with respect to the Co−C bond). Because in MeCbl and $MeCbi^+$ the methyl C $2p_z$-based MO is strongly mixed with the HOMO of the corrin macrocycle, the axial bonding interactions in these species can be inferred from the isosurface plots of the HOMOs shown in Figure 12.

This result has important implications with respect to possible Co−C bond activation mechanisms of B_{12}-dependent enzymes, as it argues strongly against models invoking involvement of the lower axial ligand. For such a mechanism to be operative, it would be necessary for the σ-donor strength of the lower axial ligand to exceed that of the alkyl ligand, in which case the central MO of MeCbl in Figure 13 would become σ-antibonding with respect to the Co−C bond (rather than the $Co-N_{ax}$ bond). However, this possibility can be ruled out because X-ray data of B_{12}-dependent holo-enzymes reveal that the lower axial position is occupied by either the DMB or a histidine residue that are considerably weaker σ-donors than alkyl ligands. Consequently, as more results become available, it seems less and less likely that enzymatic Co−C bond activation involves corrin ring deformation and/or electronic perturbations induced by the lower axial ligand. Rather, a mechanism invoking stabilization of the Co−C bond cleavage products, that is, the Co^{1+}Cbl species and the Co^{2+}Cbl/Ado$^\bullet$ radical pair in the case of MeCbl- and AdoCbl-dependent enzymes, respectively, seems more plausible.

Acknowledgment. The authors acknowledge Prof. Jorge Escalante-Semerena for useful discussions. T.C.B. thanks the University of Wisconsin, The Research Corporation (Award No. RI0596), and the NSF (CAREER grant MCB-0238530) for financial support and Dr. Frank Neese (MPI Mülheim) for supplying a free copy of the ORCA software package and for his assistance with TD-DFT computations. A.J.B. was supported by a NIH Molecular Biophysics Training Grant. N.R.B. was supported by a Howard Hughes Medical Institute Fellowship and by NIH grant GM40313 to J. C. Escalante-Semerena.

Supporting Information Available: Cartesian coordinates for all computational models, Gaussian deconvolution parameters and electronic transition analysis tables for all species studied, fit parameters for simulated Abs and RR spectra, Gaussian deconvolution figures not shown above, isosurface plots of relevant MOs for CNCbl and $MeCbi^+$, and a calculated MO diagram comparing H_2OCbl^+ to CNCbl (PDF). This material is available free of charge via the Internet at http://pubs.acs.org.

JA029328D